Coupling hydrodynamic, geochemical and isotopic approaches to evaluate oxbow connection degree to the main stream and to adjunct alluvial aquifer

Mélanie Quenet, Hélène Celle-Jeanton, Olivier Voldoire, Julie Albaric, Frédéric Huneau, Jean-Luc Peiry, Elisabeth Allain, Alexandre Garreau, Beauger Aude

HYDROL 123936

Coupling hydrodynamic, geochemical and isotopic approaches to evaluate oxbow connection degree to the main stream and to adjunct alluvial aquifer

Mélanie Quenet [(1)], Hélène Celle-Jeanton [(2)], Olivier Voldoire [(1)], Julie Albaric [(2)], Frédéric Huneau [(3,4)], Jean-Luc Peiry [(5)], Elisabeth Allain [(1)], Alexandre Garreau [(1)], Aude Beauger [(1)]

Corresponding author: Mélanie Quenet ; GEOLAB UMR 6042 UBP & CNRS - 4 Rue Ledru, 63000 Clermont-Ferrand ;

melanie.quenet@gmail.com

(1) Université Clermont Auvergne, CNRS, GEOLAB, F-63000 Clermont-Ferrand, France.

(2) Laboratoire Chrono-environnement - UMR 6249 CNRS-UFC - 16 Route de Gray, 25030 Besançon, France.

(3) Université de Corse Pascal Paoli, Faculté des Sciences et Techniques, Département d'Hydrogéologie, Campus Grimaldi, BP 52, F-20250 Corte, France.

(4) CNRS, UMR 6134, SPE, F-20250, Corte, France.

(5) Unité Mixte Internationale 3189 « Environnement, Santé, Sociétés » – CNRS UMIESS, Université Cheikh Anta Diop, Faculté de Médecine, BP 5005, Dakar Fann, Sénégal.

1. Introduction

Wetlands were subject of various scientific considerations in recent decades and benefit from specific international convention especially as waterfowl habitat (Ramsar Convention, 1971). They are indeed particularly recognized to preserve the ecological function of hydrosystems (ecological niches, refuge areas…). However, during the last decades, the general intensification of pollution has led to the contamination of most of the water bodies with negative effects on aquatic ecosystems, human health, productive activities, water system reliability and operating costs for water use (Gleick, 1998; Bates et al., 2008; Hulton, 2012; Sutton et al., 2013; UNEP, 2016). In the meantime, a world loss of about 64 to 71 % of natural wetlands is to deplore since 1900 because of human activities (Davidson, 2014). Locally, some sectors are especially affected with for instance percentage of wetlands lost reaching 91% for the California State between the 1780's to the 1980's (Dahl, T.E., 1990). Actions have been therefore implemented in order: 1) to preserve or restore wetlands, 2) to complete the knowledge on their functioning and 3) to communicate about the necessity of maintaining such environments. These are the objectives, for instance, of the 3rd National Action Plan for

Abbreviations: GW = groundwater; RB = right bank; LB = left bank; T = water temperature

Wetlands in France (PNMH, 2014) and of the United States Geological Survey (Fretwell et al. 1996).

As a special feature of wetlands, oxbows are generated by spatial and temporal dynamics of rivers within their floodplains. That kind of perifluvial environments are of a major ecological importance for the habitat and diversity of fauna and vegetation. Oxbows indeed promote reproduction and provide refuge areas for biotic communities, especially fishes (Bornette et al., 1998; Ghosh and Biswas, 2017; Yang et al., 2018). However, since an oxbow is a floodplain annex, it can be supplied by local precipitation, main stream's water, alluvial groundwater from the bank between the river and the oxbow and from the bank delineating the alluvial plain (Rollet et al., 2005). Therefore, the whole ecosystem of oxbows depends largely on hydrodynamic conditions and more peculiarly on the mixing between water masses through hydrological connectivity to the main stream and/or the alluvial groundwater (Dahm et al., 1998; Amoros and Bornette, 2002). It is now widely recognized that maintaining oxbows in riparian areas contributes to control floods occurrence, to stabilize river base flows during dry periods, to enhance the water quality (by nutrient retention) and to preserve ecosystems (Winter et al., 1998; Alard et al., 2001; Bullock and

Abbreviations: GW = groundwater; RB = right bank; LB = left bank; T = water temperature

47 Acreman, 2003; Larocque et al., 2016). However, obtain a
48 complete hydrological knowledge about oxbows' dynamic
49 remains challenging. Various monodisciplinary approaches
50 implying mostly hydrodynamic but also hydrochemistry (Carrel
51 and Juget, 1987; Bengen et al., 1992; Le Coz, 2003; Babka et
52 al., 2011; Hudson et al., 2012) have been tested separatly.
53 However, such focused investigations can lead to neglect or
54 underestimate contributions of connected water masses to
55 the whole functiunning of the oxbow which may produce
56 unaccurate conceptual models to water managers.
57 Multidisciplinary approach carried out on a representative and
58 spatially distributed sampling network (boreholes and surface
59 water points), covering both the selected wetland and the
60 connected water masses of the whole hydrosystem, constitute
61 an integrated solution to insure the most complete
62 hydrological understanding of the system and therefore
63 contribute effectively to wetlands and rivers preservation
64 actions (restoration, rehabilitation, remeandering…).

65 The present study is carried out on the Auzon Oxbow, one
66 of the fluvial annexes of the Allier River (Massif Central,
67 France, Figure 1a), located in the upper Allier River basin.
68 Ecological concerns surround that specific oxbow especially
69 since it constitutes trout's reproduction and refuge areas.

Abbreviations: GW = groundwater; RB = right bank; LB = left bank; T = water temperature

Consequently, local fishing associations carried out conservation operation as the dredging of alluvial plugs to maintain its connectivity to the main stream (Beauger et al., 2015). As an experimental site of the SOAHAL Observatory (Système d'Observation d'une Annexe Hydraulique de l'ALlier), a complete monitoring of the hydrosystem, including surface and groundwater with a dense spatial resolution (20 sampling sites for 0.4 km²) has been organized from 2014. The objectives are to provide effective diagnostic tools to evaluate the connection degree of the Auzon Oxbow to the Allier River, the main stream, and to the adjunct alluvial aquifer and thus to establish a complete hydrodynamic description of the Auzon Oxbow hydrosystem. To achieve that goal, the strategy was to combine individual investigation approaches through a multidisciplinary analysis on both hydrodynamic and hydrochemistry.

2. Study area

2.1. General settings

The study was performed on the Auzon Oxbow (sexagesimal GPS standard longitude/latitude coordinates at the confluence: 03°21’41’’E/45°22’05’’N; elevation: 400 m), a fluvial annex of the Allier River, a gravel bed meandering stream located about 60 km southeast of Clermont-Ferrand,

Abbreviations: GW = groundwater; RB = right bank; LB = left bank; T = water temperature

93 France. The Allier River originates at La Maure de Gardille
94 (1423 m.a.s.l) and joins the Loire River at the Bec d'Allier near
95 Nevers, after 410 km of course from South towards North
96 within a 14,310 km² watershed (Figure 1a). Allier River
97 discharge at the station K2430810 of Agnat (Pont d'Auzon),
98 located downstream of the study area at about 1500 m to the
99 north (03°21'26''E/45°23'09''N; elevation: 360 m), ranges from
100 9.7 to 246.0 $m^3.s^{-1}$ with an annual average at 30.3 $m^3.s^{-1}$
101 (calculated over 26 years data; ("Banque Hydro," n.d.)). The
102 Auzon Oxbow is located in the first alluvial plain encountered
103 downstream of the Allier Gorges. The study area presents a
104 temperate continental climate with relatively hot summers
105 (mean air temperatures up to 24°C in July) and cold winters
106 (mean temperatures around -3°C in February; "Météo-France"
107 n.d.). Annual precipitation is moderate within the Allier basin
108 (692 mm on average), the valley being in a shelter position
109 behind the western Massif Central where Atlantic humid air
110 masses produce orographic rainfall; most of the events occur
111 between May and October (423 mm in cumulative
112 precipitation; "Météo-France" n.d.). Mountainous areas of the
113 upper Allier catchment are more humid with a total
114 precipitation around 2000 mm; minima are registered in the
115 low Allier plain and account for around 570 mm/yr
116 (Mohammed et al., 2014).

Abbreviations: GW = groundwater; RB = right bank; LB = left bank; T = water temperature

Geologically, the drainage basin of the Allier River is composed of 80% by crystalline formations (Hercynian crystalline bedrock and Cenozoic volcanic rocks), the remaining part of the watershed is made of calcareous Oligocene fluvio-lacustrine sediments (Korobova et al., 1997). The study area is located in the small subsidence basin of Brioude. That tectonic depression constitutes the western end of an E-W direction extension grabens network due to the tectonic phase in distention which took place in Western Europe during the Cenozoic period (Vanderhaeghe and Prognon, 2012). The Brioude basement is composed of a Hercynian metamorphic and magmatic bedrock overlaid by the sedimentary formation of Limagne: during the Oligocene and Miocene periods, detrital sedimentation in continental environment (alternation of clays, sands and marls with some carbonates levels) filled the basin. Since Quaternary, the alluvial deposits of the Allier River are completing the sequence on the underlying Oligocene marls (Lasnier and Marchand, 1982; Korobova et al., 1997); they extend over a width of between 0.5 and 2 km and a thickness of about 10 m at the Auzon Oxbow site (alluvial plain of Figure 1b). Due to their good hydrodynamic properties (Transmissivity = 10^{-3} à 10^{-4} m²/s, Storage coefficient = 8 to 10%) and hydrochemical characteristics (moderate concentration, neutral pH and calcium-bicarbonate water-

Abbreviations: GW = groundwater; RB = right bank; LB = left bank; T = water temperature

type) (Mohammed, 2014; Mohammed et al., 2014), the alluvial aquifer of the Allier River is one of the major water resources of the area. This aquifer is therefore intensively exploited for drinking water supply and agricultural purposes as it is the case on the study site.

Figure 1

Thanks to its geomorphology and location, Auzon Oxbow is considered as an active floodplain oxbow (Babka et al., 2011). It was formed by the migration of an old channel of the Allier River, which occurred during two flood events in 1988 and 1989. A former gravel pit located in the point bar has facilitated the cutoff process leading to the main channel abandon. Upper part of the channel was rapidly in-filled by sands and gravels; since then, only the downstream end remains connected to the main stream (Beauger, 2008) conferring to the Auzon Oxbow the first stage of development of oxbows (Gagliano and Howard, 1984; Wren et al., 2008; Hudson et al., 2012). As so, it can be supplied by water of four different origins: local precipitation, main stream's water through the confluence, groundwater inflowing from the bank between Allier River and the oxbow and finally, groundwater from the bank delineating the alluvial plain (Rollet et al.,

Abbreviations: GW = groundwater; RB = right bank; LB = left bank; T = water temperature

2005). The 560 m length of the oxbow can be divided into three geomorphological parts (Figure 1c):

- i) the upstream zone (UZ), which is disconnected from the main stream and is similar to a pond (197 m length, 13 m width and maximum depth of 1.8 m) ;
- ii) the intermediate zone (IZ), which is a former geomorphological riffle (176 m length, 0.3 to 8 m width and maximum depth of 0.4 m) ;
- iii) and the downstream zone (DZ), which is connected to the Allier River by its downstream extremity (Beauger et al., 2015) (188 m length, 17 m width and maximum depth of 1.6 m).

Highly subject to flooding, the right bank (RB) is used for punctual grazing while the left bank (LB) is a low terrace dedicated to cereals production. However, close to the Auzon Oxbow, crops are smaller and agricultural practices relatively soft compared to the western plateau where they are much more intensive (Figure 1b). That neighboring plateau presents an aquifer that is assumed to partly feed the LB alluvial groundwater. Auzon Oxbow has been monitored since 2007 (Beauger, 2008) in terms of geomorphology, sedimentation and ecology (study of diatom, macrophyte and benthic

Abbreviations: GW = groundwater; RB = right bank; LB = left bank; T = water temperature

macroinvertebrate communities). To complete ecological investigations, the monitoring has been extended to surface and groundwater hydrodynamic and hydrochemistry. In this purpose, near-surface piezometers (from 0.92 to 1.85 m deep) were built on the oxbow's shore of both banks (Figure 1c) in 2012 (Beauger et al., 2015) as well as deep observation boreholes catching the whole aquifer thickness in 2014.

2.2. Sampling sites

Precipitation height have been collected from Météo-France database at Sainte-Florine, the closest weather station, located 4 km north-west (03°19'00''E/45°24'00''N; elevation: 450 m; station 43185001) and at Naussac (03°49'42''E/44°44'54''N; elevation: 967 m; station 48105001), weather station characterizing the upper part of the Allier watershed. Allier River daily discharge is taken from the Agnat-Pont d'Auzon station ("Banque Hydro," n.d.).

In addition, monthly monitoring is performed at the following sites in the area (Figure 1): i) 6 surface water observation points distributed along the entire Auzon Oxbow from its upstream to its downstream ends (B2 to B7); ii) 1 surface water observation point in the Allier River (Allier); iii) 6 observation boreholes (10 m deep covering the entire alluvial aquifer thickness), 2 drilled in the Right Bank (RB: PZ1 and PZ2)

Abbreviations: GW = groundwater; RB = right bank; LB = left bank; T = water temperature

and 4 in the Left Bank (LB: PZ3 to PZ6); iv) 7 near-surface piezometers (0.85 to 1.92 m deep), located next to the oxbow on both RB and LB (P2 to P9); v) Le Monteil spring (Figure 1b) draining the neighboring plateau aquifer, which is assumed to partly feed the alluvial groundwater.

3. Sampling and analytical methods

3.1. Hydrodynamic monitoring [07/22/2014 – 11/24/2017]

In order to assess the hydrodynamic behavior of the oxbow, the potential water sources entering the system have been investigated in terms of hydrodynamic and hydrochemistry. Surface water level of the Allier River at the confluence with the Auzon Oxbow and water table in the 6 observation boreholes have been recorded on an hourly basis with an in situ Level Troll 500 probe. All water level data have been corrected from the barometric pressure variations. The hydrological station was located on LB prior to the 11/05/2015 (A1, Figure 1c) and then moved to RB (A2, Figure 1c) because of a too important erosion of the left bank during previous floods. Geographical coordinates and elevation of each pressure sensor were measured using the centimetric Trimble R10 DGPS whose data was post-processed with Trimble

Abbreviations: GW = groundwater; RB = right bank; LB = left bank; T = water temperature

232 Business Center software (version 3.8.) and adjusted according
233 to the dimensions of the boreholes in order to calculate level
234 variations through time in the same reference of altitude
235 (Cunningham and Schalk, 2011). The reliability of the
236 continuous piezometric levels monitoring was checked and
237 validated through manual measurements carried out during
238 the 40 sampling campaigns: correlation coefficients between
239 data recorded and manually measured (r^2 from 0.92 to 0.99)
240 testify for a good representativeness of the piezometric level
241 time-series.

242 ***3.2. Water chemistry monitoring***

243 Forty sampling campaigns have been performed on the 21
244 sampling sites on a monthly basis from July 2014 to November
245 2017, except in February 2017 when the alluvial plain was
246 flooded. A few data are also missing for P7, because of small
247 floods or vandalism. Prior to sampling, bottles have been
248 rinsed two times by using the water to be sampled. Surface
249 waters and Le Monteil spring were directly sampled using
250 sampling vials. Groundwater was sampled using a Cole Parmer
251 Masterflex I/S pump for near-surface piezometers, while it was
252 a 12 V standard PVC narrow diameter submersible pump for
253 the observation boreholes. For each groundwater sampling,
254 stagnating water present into the borehole was renewed

Abbreviations: GW = groundwater; RB = right bank; LB = left bank; T = water temperature

255 before sampling and measuring. An intensive campaign was
256 performed on the 23rd of November 2017 in the Auzon Oxbow
257 in order to assess spatial distribution of electrical conductivity
258 (EC): 124 measures have been performed in the near surface
259 of the oxbow (0.2 m depth) along the UZ, the IZ and on the
260 upper part of the DZ, using a WTW multi 340i and a DGPS
261 Trimble Geo7x whose data were post-processed with
262 Pathfinder software. Two sites of the EC campaign (Points 3
263 and 103) were also sampled for major ions analyses. EC, pH
264 and temperature have been measured in situ using a WTW
265 multi 340i. HCO_3^- concentrations have been determined
266 directly in the field by using HACH Digital Titrator, sulfuric acid
267 (0.1600 N and 1.600 N) and Bromocresol Green-Methyl Red
268 Indicator (Hach method 8203).

269 A total of 837 water samples have thus been taken in clean
270 sterile polypropylene straight containers with polyethylene
271 caps of 180 mL, transported in cooler to GEOLAB laboratory in
272 Clermont-Ferrand (CNRS UMR 6042, University Clermont-
273 Auvergne) and then stored at 4°C. Anions and cations were
274 analyzed within 3 days in GEOLAB Laboratory: anions (F^-, Cl^-
275 NO_2^-, NO_3^-, PO_4^{3-}, SO_4^{2-}) using the Thermo Fisher Scientific
276 Dionex DX120 ionic chromatography with a Ionpac AS23 4*250
277 mm column and the Dionex 7 anions standard solution;

Abbreviations: GW = groundwater; RB = right bank; LB = left bank; T = water temperature

cations (Li^+, Na^+, NH_4^+, K^+, Mg^{2+}, Ca^{2+}) using the Thermo Fisher Scientific Dionex ICS1100 ionic chromatography with a Ionpac CS12A 4*250 mm column and the Dionex 6 cations standard solution. The error margins were of ± 4-6% and ±2-4% respectively for anions and cations. These analyses are reliable since all the 839 ionic balances (837 monthly + punctual samples 3 and 103) are under 10% with even 95.1% under 5%.

From July 2014 to March 2017, only groundwater from the six observation boreholes has been analyzed for stable isotopes. Since April 2017, all sites have been sampled for δ^2H and $\delta^{18}O$ analyses, so the database accounts for 360 isotopic analyses. Waters have been collected with no air bubbles, in 20 mL borosilicate glass vials closed by polypropylene caps. Isotopic analysis were performed at the University of Corsica, France (CNRS UMR 6134 SPE): both ^2H and ^{18}O of the water molecule were characterized using a liquid-water stable isotope analyzer DLT-100 (Los Gatos Research) according to the analytical scheme recommended by the IAEA (IAEA, 2009; Penna et al., 2010). Isotopic data were reported in the standard delta notation in part per thousand relative to Vienna Standard Mean Ocean Water (VSMOW; (Clark and Fritz, 1997)). The accuracy is 1‰ for δ^2H and 0.1‰ for $\delta^{18}O$.

Abbreviations: GW = groundwater; RB = right bank; LB = left bank; T = water temperature

3.3. Geophysical investigations

Electrical Resistivity Tomography (ERT) is a geophysical method providing images of electrical resistivity ρ (inverse of conductivity) of the subsurface. ERT is generally used to characterize the lithology and the geometry of the ground, to assess its saturation, or even to monitor soil pollution (Loke, 2011). The technique consists of injecting current in a pair of electrodes set into the ground and measuring the resulting potential difference between another dipole of electrodes which yields information about ρ.

A 2D ERT survey was carried out on the SOAHAL Observatory on the 02/21/2018 in order to investigate potential underground connections between Auzon Oxbow and Allier River. The data collection was done by using a SYSCAL R1+ (Iris instruments), with a Wenner-Schlumberger electrode configuration (Loke and Barker, 1996). An array of 72 electrodes was installed, distributed every 3 m, along a NNW-SSE line (Figure 1c). The apparent resistivity data were inverted with RES2DINV software (Loke, 2016) using least-squares inversion optimization. Inversion converged to RMS error of 3% after 5 iterations.

4. Results and discussion

Abbreviations: GW = groundwater; RB = right bank; LB = left bank; T = water temperature

4.1. End-members characterization and interactions

4.1.1. Hydrodynamical data

Allier River discharge presents an average value of 25 $m^3.s^{-1}$ for the studied period (07/22/2014 – 11/24/2017). The most important flood impulse reached 328 $m^3.s^{-1}$ (11/23/2016) while two other flood peaks have been registered equal or superior to 150 $m^3.s^{-1}$ (156 $m^3.s^{-1}$ on the 11/29/2014 and 150 $m^3.s^{-1}$ on the 04/06/16; Figure 2d). These events are quite moderate compared to the large floods that Allier River can historically experience (10Y-flood and 50Y-flood: 590 and 840 $m^3.s^{-1}$ respectively; Banque Hydro, n.d.). Annual discharge variations are observed with globally low flow (LF) periods during the warmest months (from July to October) with an average flow rate around 14 $m^3.s^{-1}$ while high flow (HF) periods including important flood events occur along the rest of the year with an average flow rate around 32 $m^3.s^{-1}$. This LF-HF distribution over time is more consistent with variations of precipitation recorded in the upstream mountainous area (Mohammed et al., 2014), whose Naussac weather station is the witness (Figure 2a), than the local ones (represented by Sainte-Florine weather station on Figure 2a). However, the maximum flood peak of 328 $m^3.s^{-1}$ is actually related to high

Abbreviations: GW = groundwater; RB = right bank; LB = left bank; T = water temperature

345 precipitation recorded at both stations, suggesting a
346 generalized rainfall event linked to a Cevénol episode (a
347 climatic phenomenon more and more frequent these last few
348 years with rainy events that mainly affects the Cevennes'
349 mountain range and piedmont which often cause severe
350 floods in the Massif Central Region) (Jubertie, 2006; Gay,
351 2015). On the contrary, flood peak occurring the 01/26/2017
352 seems to be only due to high altitude precipitation: rainfall
353 event is actually only recorded at Naussac weather station.
354 Finally, flood peak recorded the 08/30/2017 is caused by a
355 stormy event affecting Saint-Florine weather station only.
356 These examples emphasize that discharge variations recorded
357 for Allier River are related to a large set of meteorological
358 conditions affecting the entire Allier basin, including rapid
359 winter temperature elevation with or without rainfall causing
360 snow melting (Jubertie, 2006).

361

362 **Figure 2**

363

364 Water level variations at the Auzon Oxbow/Allier River
365 confluence (solid black lines in Figure 2b and Figure 2c) are
366 consistent with discharge variations of the Allier River
367 recorded at Agnat-Pont d'Auzon station (Figure 2d). It shows

Abbreviations: GW = groundwater; RB = right bank; LB = left bank; T = water temperature

368 the accuracy of the *in situ* surface water level monitoring
369 which was therefore crossed with water table monitoring for
370 piezometric mapping (triangular interpolation). Figure 3a and
371 Figure 3b present LF (08/04/2015) and HF (04/06/2016)
372 piezometric maps, respectively. These two dates are identified
373 on Figure 2d. The LF piezometric map indicates a global
374 northward circulation of groundwater (GW) and identified GW
375 as a potential end-member supplying Auzon Oxbow. Water
376 level time-series observation (Figure 2b and Figure 2c) shows
377 that PZ1 and PZ2 (RB) as well as PZ4 (LB) present very
378 impulsive variations. They were pretty close to the water level
379 variations at the confluence Auzon Oxbow/Allier River.
380 Moreover, in HF, piezometric levels were lower than surface
381 water levels with 0.7% of the records at PZ1, 0.3% at PZ2 and
382 4% at PZ4. This observation suggests that GW are supplied by
383 surface water, whatever bank considered, during HF. PZ3, PZ5
384 and PZ6 (LB) show smoother signals (Figure 2b); most of the LB
385 piezometric level variations remained consistent with the
386 surface water level variations.

387

388 **Figure 3**

389

Abbreviations: GW = groundwater; RB = right bank; LB = left bank; T = water temperature

390 The HF piezometric map illustrates the hydrodynamic situation
391 during the third most important flood event of the studied
392 period. This flood was linked to a large rainfall event which
393 affected the whole Allier River catchment (Figure 2a). The map
394 can be used to identify potential hydrodynamic changes
395 compared to LF situation. Then an inversion of the hydraulic
396 gradient is induced by high surface water level recorded at the
397 Auzon Oxbow/Allier River confluence; it affects GW on both
398 Auzon Oxbow banks. However, in the RB, inversion is reduced
399 to a GW flow inversion (from PZ2 to PZ1) since the Allier River
400 discharge just began to decline while the RB is still in charge.
401 On the LB, inversion seemed to extend from surface water to
402 PZ5 passing through PZ4. Actually, during that HF event as
403 generally for all HF recordings, PZ4 levels varied synchronously
404 with the surface water level up to inversion of hydraulic
405 gradient while the other LB boreholes remained stable, PZ5
406 included. PZ3 piezometric level starts to increase only 24h
407 after the rise of surface water level, the response delay of PZ5
408 and PZ6 is about 26h. Besides, PZ5 piezometric level stays
409 lower than the one of PZ6, inducing a piezometric depression.
410 The delay between the increase in surface water level and that
411 of the more inland LB boreholes suggests that the hydraulic
412 gradient inversion is limited to PZ4. This hydrodynamic feature
413 can be explained by high disparities existing within the alluvial

Abbreviations: GW = groundwater; RB = right bank; LB = left bank; T = water temperature

414 deposits (from silts to gravels; Teles et al., 2004; Ounaïes et al.,
415 2013; Sarris et al., 2018). These 3D heterogeneities lead to
416 variations in water flows distribution within the aquifer.

417 To summarize, hydrodynamic data highlight that during LF,
418 Auzon Oxbow is supplied by GW. During HF, an inversion of
419 the hydraulic gradient is recorded and Auzon Oxbow
420 contributes to the recharge of GW. RB is entirely concerned by
421 this recharge while only the oxbow closest borehole (PZ4) is
422 affected in the LB (Figure 3b). The important time delay
423 observed between surface water flood peaks and GW
424 recharge at PZ3, PZ5 and PZ6 (from 24 to 26h) indicates that
425 LB GW is mainly recharged by the southern GW system.

426

427 *4.1.2. Physico-chemical data*

428

429 For the 21 sample sites, physico-chemical parameters
430 measurements (water temperature – T; pH; electrical
431 conductivity – EC) as well as ions concentrations and water
432 stable isotopes determinations are presented in Table 1 with
433 average (arithmetic means), minimum, maximum and
434 standard deviation values. EC vs T data of the entire SOAHAL
435 observatory are reported in Figure 4a while EC time-series of
436 Auzon Oxbow DZ (B2bis), IZ (B4), UZ (B7) and of each end-

Abbreviations: GW = groundwater; RB = right bank; LB = left bank; T = water temperature

437 member are quoted in Figure 4b: Allier River, PZ1 (RB GW),
438 PZ3-PZ4 (LB GW with an increasing distance to the Auzon
439 Oxbow from PZ4 to PZ3).

440 The pH values are comprised between 6.5 and 8.8 (Table
441 1), which is consistent with natural water pH usually ranging
442 from 6.5 to 9.5. The more neutral values have been recorded
443 in GW and are assumed to be due to the buffering capacity of
444 soils. EC and T values were the most interesting physico-
445 chemical parameters to differentiate water end-members
446 (Figure 4):

447 - Allier River EC is the lowest one within the study site
448 (110 ± 17 µS.cm^{-1}; Table 1), without any significant
449 variations during the year (Figure 4b). On the contrary
450 T experiences high amplitudes (from 0.9 to 21.8°C;
451 Table 1) as an impact of air temperature annual
452 variation.
453 - PZ1 and PZ2 show the lowest EC values of the
454 boreholes (with 290 and 491 µS.cm^{-1} respectively;
455 Table 1). EC annual variations are relatively low (Figure
456 4b) while T amplitudes can reach more than 12°C
457 (Table 1). The RB (P2, P4, P6, and P9) and LB (P7) near-
458 surface piezometers (Figure 1c) also present low EC
459 values and high T amplitudes (Figure 4a and Table 1).

Abbreviations: GW = groundwater; RB = right bank; LB = left bank; T = water temperature

460 - PZ3 to PZ6 are characterized by the highest EC values
461 (mean value of the four boreholes: 981 µS.cm^{-1}) while T
462 experienced the smaller variations (around 7°C; Table
463 1). EC time-series show a quite stable signal with no
464 clearly identified seasonal variations (Figure 4b). P3
465 and P5, the two remaining LB near-surface piezometers
466 (Figure 1c) present similar EC and T patterns (Figure 4a
467 and Table 1).
468 - Le Monteil spring shows a high EC value (925 µS.cm^{-1},
469 Table 1) and low amplitude of T (6.7°C; Table 1) which
470 is consistent with the LB GW (Figure 4a).

471

472 **Table 1**

473

474 **Figure 4**

475

476 *4.1.3. Hydrochemical data*

477

478 Hydrochemical data of Table 1 have been plotted on a
479 Piper diagram (Figure 5) in order to define the geochemical
480 water-types of each end-member. Water types are distributed
481 between two groups with a noticeable difference in the
482 cations content. The first group has a Ca-Na/HCO_3 type and

Abbreviations: GW = groundwater; RB = right bank; LB = left bank; T = water temperature

483 includes Allier River, PZ1-PZ2 (RB GW), P2-P4-P6-P9 (RB near-
484 surface piezometers), P7 (LB near-surface piezometer) and
485 then the second group presents a Ca/HCO_3 signature and
486 corresponds to PZ3 to PZ6 (LB GW), P3 and P5 (the two
487 remaining LB near-surface piezometers) and Le Monteil Spring.
488 Then, the GW signal shows a clear distribution between RB
489 and LB. RB GW are predominantly supplied by Allier River
490 whereas LB GW chemical facies is consistent with the one of
491 the plateau aquifer (Le Monteil). This is in agreement with
492 hydrodynamic data. P7 can be quoted as an exception to this
493 RB/LB GW distribution, as this LB near-surface piezometer
494 presents physico-chemical and geochemical characteristics
495 close to the RB GW ones.

496 Chemical difference between Allier River (as well as RB
497 GW) and LB GW is due to the geological composition of the
498 watershed. Actually, the $Ca\text{-}Na/HCO_3$ water type of the Allier
499 River can be related to the volcano-metamorphic basement:
500 upstream of the study site, the Allier River incised the
501 basement while downwards, the riverbed widens within the
502 Brioude basin where an enrichment in calcareous nodules
503 between Vieille Brioude and the study site has been
504 documented (Lasnier and Marchand, 1982). Carbonate
505 dissolution occurrences are reported in the Allier River and the

Abbreviations: GW = groundwater; RB = right bank; LB = left bank; T = water temperature

506 shallow GW associated (Négrel et al., 2004). Sodium minerals,
507 subjects to weathering, are reported as common in the Allier
508 terraces, as augite, green and brown hornblende and
509 nepheline (Rudel, 1963; Pastre, 1986; Veldkamp and
510 Jongmans, 1990), which explain the Na-enriched signature of
511 the Allier River and so that of the RB GW. The Ca/HCO_3 water
512 type of LB GW has been already described by several authors
513 (Négrel et al., 2004; Vanderhaeghe and Prognon, 2012;
514 Mohammed et al., 2014) and corresponds to many alluvial
515 aquifers in France (Roux, 2006) and over the world (Chkirbene
516 et al., 2009; Andrade and Stigter, 2011; Huang et al., 2014).
517 Indeed, because the mineral phases that composed alluvial
518 aquifers do not generally impose a very marked geochemical
519 type and because of short residence times within the aquifer,
520 alluvial GW presents frequently a Ca/HCO_3 water type (Roux,
521 2006).

522

523 **Figure 5**

524

525

Abbreviations: GW = groundwater; RB = right bank; LB = left bank; T = water temperature

4.2. Auzon Oxbow as a result of the mixing between end-members

4.2.1. General features of Auzon Oxbow chemistry

In a first approximation, taking into account their origin, perifluvial oxbows and main stream are supposed to have a similar chemical composition (Négrel et al., 2003). However, despite its still active connection with the Allier River, the Auzon Oxbow presents a mean EC value (300 $\mu S.cm^{-1}$) higher than Allier River one (110 $\mu S.cm^{-1}$) but lower than GW (784 $\mu S.cm^{-1}$ in mean for observation boreholes of both banks). This indicates that the Auzon Oxbow water results from a mixing between the low concentration water of the Allier River and the more concentrated one of GW, whatever the bank (Table 1, Figure 4). Figure 6 confirms this trend and highlights a clear evolution of the Auzon Oxbow between a Na-pole characterized by Allier River and a more calcic end member delineated by LB GW. RB GW water type is close to the Auzon Oxbow one and seems to result also from the mixing between Allier River and LB GW. The proximity of LB GW and Le Monteil spring confirms the contribution of the plateau aquifer to the alluvial GW. This general feature is however not constant within the hydrological cycle: records of April 2016

Abbreviations: GW = groundwater; RB = right bank; LB = left bank; T = water temperature

549 (highlighted by the grey area of Figure 4b) show a decrease of
550 Auzon Oxbow EC which reaches the value of Allier River. This
551 specific period corresponds to one of the major floods that
552 have affected the Allier River during the study, with a
553 discharge flow of 150 $m^3.s^{-1}$ registered on the 04/06/16 (Figure
554 2d). During this period, the Allier River penetrated further into
555 the Auzon Oxbow. This surface water arrival, characterized by
556 a low concentration, affected the Auzon Oxbow up to B6, B7
557 showing constant EC. This was a short-time process since
558 Auzon Oxbow recovered its pre-flood concentration the
559 month after (Figure 4b), indicating that the oxbow restitutes
560 quickly to the main stream what it absorbs during flood. This
561 time-constrain phenomenon has already been quoted for
562 oxbows by Carrel and Juget, (1987) for the Morte du Sauget,
563 one of the Rhône oxbows and for oxbows of Ain River (Le Coz,
564 2003). PZ4 records also an EC decrease in April 2016, in
565 accordance with the inversion of the hydraulic gradient
566 showed in HF piezometric map (Figure 3b).

567

568 **Figure 6**

569

570

571

Abbreviations: GW = groundwater; RB = right bank; LB = left bank; T = water temperature

572 *4.2.2. Identification of punctual arrivals of GW within Auzon*
573 *Oxbow*
574
575 To precise the downstream-upstream evolution within the
576 Auzon Oxbow, a fine cartography of EC has been performed on
577 the 11/23/2017, during a low flow stage (Allier River daily
578 discharge: 6.7 $m^3.s^{-1}$). Figure 7 presents the results of this
579 campaign and puts in evidence a difference between the
580 upstream zone characterized by low EC values, mainly in the
581 range 0-250 $\mu S.cm^{-1}$, and IZ and DZ parts of the Auzon Oxbow
582 with values comprised between 250 and 400 $\mu S.cm^{-1}$. This
583 general pattern is disturbed by local arrivals of water. A high
584 EC is observed along the downstream zone left bank (point
585 103 = 735 $\mu S.cm^{-1}$; Figure 7) and testifies for a high
586 concentration groundwater arrival. On the contrary, the whole
587 upstream part is characterized by low EC in accordance with
588 low concentration water incomes, some of which were
589 identified as coming from the bed of the oxbow. Points 3 (as
590 an example of the latter) and 103 have been sampled for ions
591 analyses.
592
593 **Figure 7**
594

Abbreviations: GW = groundwater; RB = right bank; LB = left bank; T = water temperature

595 Physico-chemical parameters and ions concentrations of
596 samples acquired on the 11/23-24/2017 for the points 3, 103
597 and the 21 followed sites are reported in Table 2. Results show
598 that:

599 - Point 103 presents a Ca/HCO_3 signature pretty close to
600 that of LB GW (Figure 8) and especially PZ4 (Table 2,
601 Figure 8). PZ4 shows higher NO_3^- (13.1 $mg.L^{-1}$) probably
602 due to a contamination of alluvial GW, but not
603 transmitted or degraded before the transfer LB GW to
604 Auzon Oxbow.
605 - The low concentration water arrival located at the UZ
606 end of the oxbow (Point 3) presents a $Ca\text{-}Na/HCO_3$
607 water type similar to Allier River one (Table 2, Figure
608 8). This is in accordance with an upstream supply by
609 the Allier River. The water arrival of Point 3 was coming
610 from the bed of the oxbow which indicates that this
611 supply is realized through underground inflows. The
612 location of these low concentration water arrivals
613 directly close to the paleochannel visible in the
614 landscape, suggests that an old and deeper channel
615 connects Auzon Oxbow to Allier River. The potential
616 recharge by underground paleochannels, because of
617 their high hydraulic conductivity, has already been
618 observed (Rathore et al., 2010; Babka et al., 2011).

Abbreviations: GW = groundwater; RB = right bank; LB = left bank; T = water temperature

Table 2

Figure 8

Therefore, to verify the present hypothesis, an ERT sounding has been performed on the 02/21/2018 (high flow period, Allier River daily discharge = 57.3 $m^3.s^{-1}$, see part 3.3). The location of the profile is indicated in Figure 1c. Oriented SSE-NNW, the profile was designed perpendicularly to the visible paleochannel and close to the upstream end of the Auzon Oxbow. Indeed, electrical resistivity sounding has already been used to investigate subsurface paleochannel geometry, architecture and hydrodynamic (Sinha et al. 2013) as well as fresh GW discharge through a paleochannel (Kolker et al., 2013). The resulting ERT profile indicates a general decrease of the electrical resistivity with depth (Figure 9). Two main zones can however be observed. In the first one, from surface to 8-10 m depth, resistivity varies laterally. The southern part of the profile, along with the 48 first lateral meters on Figure 9, presents a relatively low resistivity (ρ = 150 to 350 $\Omega.m^{-1}$) compared to the rest of the section (ρ > 600 $\Omega.m^{-1}$). It can be interpreted as a sand formation saturated

Abbreviations: GW = groundwater; RB = right bank; LB = left bank; T = water temperature

642 with freshwater (Sinha et al., 2013). This is consistent with the
643 presence of the paleochannel of the Allier River (Figure 1c),
644 which higher porosity induces lower resistivity (Archie, 1942).
645 In addition, there is lateral resistivity change within the
646 paleochannel which most likely reflects the progressive filling
647 of the system and a potential connection to the river (blue
648 circle on Figure 9). The second zone starts below 10 m depth
649 with low resistivity values and corresponds to the Oligocene
650 marl substratum (Lasnier and Marchand, 1982; Korobova et
651 al., 1997).

652

653 **Figure 9**

654

655 This paleochannel supplies the Auzon Oxbow with low
656 concentration water and explains the low EC and the water
657 types observed in the upstream part of the Auzon Oxbow and
658 in the near-surface piezometer P7 (Figure 1c). The repartition
659 of Auzon Oxbow points along the mixing line of the Figure 6,
660 with B7 closer to the Allier River end-member than B2 is thus
661 explained. For information, a simple estimation of contribution
662 percentages of Allier River and LB GW to the oxbow (at its
663 different sampling locations) can therefore been deduced
664 from the Figure 6 data. Indeed, considering that the chemical

Abbreviations: GW = groundwater; RB = right bank; LB = left bank; T = water temperature

665 characteristics of the Allier River end-member point (30.2 mg.l^{-1}
666 of HCO_3^- and a Na/Ca ratio of 0.95) represent 100% of
667 contribution from the main stream and that those of LB GW
668 (302.6 mg.l^{-1} of HCO_3^- and a Na/Ca ratio of 0.23) represent 0%,
669 it is easy to deduce the contributions of those end-member to
670 the oxbow at the different sampling sites. So, it was logically
671 estimated that B2, the closest location to the confluence and
672 B7, the closest location to the paleochannel arrival, were
673 mostly and equally fed by the Allier River with respectively 63
674 and 64 % of contribution. The rest of the oxbow would be,
675 according to these strictly indicative estimates, as much fed by
676 the river as by the alluvial groundwater (49 % of Allier River
677 contribution for B3, 50 % for B4 and 51 % for B2bis and B6).
678 Those estimates would imply that alluvial groundwater
679 contributions to the Auzon oxbow are not negligible and that,
680 in terms of contribution share, the river contributes as much
681 by the confluence as by the upstream paleochannel to the
682 oxbow water supply.

683

684 4.*2.3. Use of δ^2H and $\delta^{18}O$ of the water molecule for temporal*
685 *insight*

686

Abbreviations: GW = groundwater; RB = right bank; LB = left bank; T = water temperature

687 The ^{2}H-^{18}O stable isotopes of the water molecule
688 constitute one of the best water tracer since it provides
689 information about water origins as well as water mixing
690 processes through the hydrological cycle (Fontes, 1980; Clark
691 and Fritz, 1997; Kendall and McDonnell, 1999). For the study
692 of wetlands, they allow approaching their functioning (Hunt et
693 al., 1998; Clay et al., 2004) and more peculiarly to characterize
694 the isotopic content of the different supplying sources or the
695 Auzon Oxbow (Babka et al., 2011) according to the
696 temperature-, amount-, altitudinal- and continental-effects
697 (Rozanski et al., 2001).

698 For coherent interpretations, data from April to November
699 2017, period of the concomitant investigation of all sites, have
700 been selected among the database. Allier River (-8.0 $\delta^{18}O$‰, -
701 52.0 $\delta^{2}H$‰) and RB GW (-8.1 $\delta^{18}O$‰, -53.2 $\delta^{2}H$‰) present the
702 most depleted isotopic content. The LB GW (-7.7 $\delta^{18}O$‰, -51.5
703 $\delta^{2}H$‰) and Le Monteil spring (-7.3 $\delta^{18}O$‰, -50.0 $\delta^{2}H$‰) are
704 characterized by more enriched signatures. As previously
705 referred by Négrel et al. (2003) and by Mohammed et al.
706 (2014), Allier River displays a clear seasonal variation (Figure
707 10a) with depleted values during winter and more generally
708 during HF period (around -8.5 $\delta^{18}O$‰) than for summer
709 (around -7.5‰), mainly due to the temperature effect on

Abbreviations: GW = groundwater; RB = right bank; LB = left bank; T = water temperature

precipitation. Figure 10b shows δ^2H_{VSMOW} (‰) vs $\delta^{18}O_{VSMOW}$ (‰) means for Auzon Oxbow sampling sites and its end-members. Taking into account the high variability of the Allier River data, all the measurements have been plotted individually. Precipitation is represented by the Global Meteoric Water Line (GMWL) of Craig (1961), and more regionally by the Local Meteoric Water Line (LMWL) proposed by Petelet-Giraud et al. (2005) with a local average of $\delta^2H = 8* \delta^{18}O + 13.7$‰ and low altitude rainfalls of Cournon (03°13’33’’E/45°44’54’’N; elevation: 327 m; period 2013-2016; AUVERWATCH Database, 2018; Celle-Jeanton, 2017). All data follow a trend line between LMWL and local precipitation of Cournon rainfall, the more depleted signal is characterized by the samples of Allier River during HF (-8.5 $\delta^{18}O$‰, -55.0 δ^2H‰) while the more enriched by the Allier River LF ones (-7.4 $\delta^{18}O$‰, -49.1 δ^2H‰), LB GW (-7.7 $\delta^{18}O$‰, -51.5 δ^2H‰) and Le Monteil spring (-7.3 $\delta^{18}O$‰, -50.0 δ^2H‰). Allier River HF data follow the LMWL and are representative of the colder and higher altitude precipitation. The more enriched and evaporated signal of Allier River LF is explained by low altitude precipitation (summer local storms) and/or local GW supply. This is consistent with the previous conclusions based on hydrodynamic data that showed relationships between low flow surface water and groundwater, with more enriched GW

Abbreviations: GW = groundwater; RB = right bank; LB = left bank; T = water temperature

734 during summer, due to evaporation process (Geyh and Mook,
735 2000; Mohammed et al., 2014). Auzon Oxbow isotopic data
736 are well plotted along a mixing line between Allier River HF
737 and isotopically enriched waters. Auzon Oxbow DZ (B2 and
738 B2bis) presents the more enriched and evaporated signal close
739 to that of the LB GW; the heavy isotopes content globally
740 decreases up to the UZ (B7; Figure 10b). On a temporal scale,
741 evolution of isotopic data in the Auzon Oxbow tends to
742 homogenize and the 3 identified zones DZ (B2bis), IZ (B4) and
743 UZ (B7) present, in winter period, the same isotopic content
744 (Figure 10a). This behavior is partly explained by previous
745 observations: DZ is subject to a double supply through its
746 connection to the Allier River at the confluence and LB GW
747 inputs (Point 103). The later explains the more enrich isotopes
748 contents and its important variations through time. B7 has
749 been shown to be supplied by Allier River that inflows to the
750 Auzon Oxbow through the subsurface paleochannel. However,
751 B7 presents a behavior completely different from the one of
752 Allier River and isotopic values of B7 match only the Allier
753 River ones during winter high flow period (Figure 10a). This
754 observation provides precision about the recharge of the
755 Auzon Oxbow from the paleochannel that occurs only
756 seasonally, during HF periods, as for the RB GW. Indeed,
757 according to the hydrodynamic monitoring, the RB GW

Abbreviations: GW = groundwater; RB = right bank; LB = left bank; T = water temperature

758 recharge through inversion of the hydraulic gradient during HF
759 which is also in agreement with the depleted isotopic values
760 observed for RB GW.

761

762 **Figure 10**

763

764 ***4.3. Conceptual model of the Auzon Oxbow***

765 The multidisciplinary analysis between hydrodynamic,
766 geochemical and isotopic approaches carried out at the dense
767 SOAHAL Observatory allows establishing a reliable conceptual
768 model of the hydrodynamical functioning of the Auzon Oxbow
769 (Figure 11). As expected for that kind of perifluvial
770 environments (Rollet et al., 2005), interactions between the
771 oxbow and both the main stream and the alluvial aquifer were
772 identified. Since the Auzon Oxbow is disconnected from the
773 main stream in its upstream end for the last 30 years, the
774 Allier River supplies the oxbow generally through the
775 downstream confluence (surface water flows on Figure 11).
776 However, during major flood events the main stream can
777 submerge the right bank and then supply the entire oxbow
778 area. Geochemical data show another interaction between the
779 Allier River and the Auzon Oxbow, through the upstream
780 underground paleochannel, recognized both via geochemical

Abbreviations: GW = groundwater; RB = right bank; LB = left bank; T = water temperature

781 analysis and geophysical investigations. A detailed isotopic
782 analysis has shown that this Auzon Oxbow area has a similar
783 isotopic signature than Allier River during high flow periods
784 only. This observation implies that the paleochannel is active
785 from November to June only. This is in agreement with the
786 results of hydrodynamic and geochemical approaches which
787 identified existing pathways from surface water to alluvial
788 groundwater during the same periods (high flow GW flows on
789 Figure 11).

790

791 **Figure 11**

792

793 The coupling approach also testifies for a supply of the
794 oxbow by the alluvial groundwater, this especially affects the
795 water composition in its downstream part. As this part of the
796 oxbow is the site of its confluence to the Allier River,
797 groundwater supply could have been underestimated
798 otherwise. That connection with the adjunct alluvial aquifer is
799 active during low flow (Figure 11). LB GW are mainly supplied
800 by the southern part of alluvial aquifer and the neighboring
801 agricultural plateau (permanent GW flows on Figure 11),
802 except during high floods when small gradient inversions can
803 drive pathways from surface water to groundwater.

Abbreviations: GW = groundwater; RB = right bank; LB = left bank; T = water temperature

804 The active connection existing between the Auzon Oxbow
805 and the Allier River through the underground paleochannel
806 would not have been identified and specified without the
807 geochemical and isotopic approaches. A standard
808 hydrodynamic study based on their apparent
809 geomorphological surface connection would have produced an
810 incomplete understanding of the Auzon Oxbow hydrosystem.
811 Besides, while studies attest for the importance of oxbow
812 connection degree to the main stream on the water quality
813 (Carrel and Juget, 1987; Bengen et al., 1992), it is mostly based
814 on the type of surface connection observed between the two
815 water bodies (oxbow isolated from the river or connected
816 through one or two sides as Ward et al. (2002) described).
817 Those observations indeed inform about the extent of the
818 hydrological connection that impacts the water chemistry of
819 oxbows (Tockner et al., 1999; Glińska-Lewczuk, K., 2009)
820 especially for instance for metals contaminations (Ciazela et
821 al., 2018). However, the present study show that consequent
822 underground connection can also occur between the main
823 stream and the oxbow through paleochannel as already
824 suggested by Babka et al. (2011), increasing so their apparent
825 connection degree and impacting the water chemistry of the
826 oxbow. Therefore, the possibility of underground connectivity
827 to the main stream should be further considered in oxbows

Abbreviations: GW = groundwater; RB = right bank; LB = left bank; T = water temperature

828 hydrogeological studies. Applying multidisciplinary approach
829 as the one performed on the Auzon Oxbow should so be
830 essential to the establishment of reliable conceptual models
831 and to their resulting management applications.

832

Abbreviations: GW = groundwater; RB = right bank; LB = left bank; T = water temperature

5. Conclusions

In a near future, wetlands like oxbows are assumed to become more and more determinent as nature-based solutions to respond to hydrological (river discharge control) and ecological (excess nutrients removal function) concerns. Therefore, the dynamic of these specific hydrosystems must be fully understood. However, the establishment of complete and usefull functionning models is complicated by the different connection degrees that can have these specific wetlands with the surrounding water masses. The task is all the more difficult since it is usually undertaken through individual investigation approach which can neglect or underestimate some supply components. The objectives of the present study were so to provide effective diagnostic tools to evaluate oxbow connection degree to the main stream and to the adjunct alluvial aquifer in order to be able to establish a complete hydrodynamic description of such hydrosystems.

The Auzon Oxbow conservation is the subject of local/regional great concerns especially for the local fishing associations. In fact, hydrodynamic and hydrochemical features of Auzon Oxbow have a direct impact on its ecological functions as reproduction and refuge areas for emblematic fishes such as trouts. This study so proposed the coupling of hydrodynamic,

Abbreviations: GW = groundwater; RB = right bank; LB = left bank; T = water temperature

geochemical and isotopic approaches to produce a model which can serve as a reference state for further operations of conservation and management of the Auzon Oxbow. The conceptual model thus produced attests to a greater degree of connection than expected between the Auzon Oxbow and both the main stream and the alluvial aquifer. Indeed, despite their surface upstream disconnection for the last 30 years, the study proved that Allier River supplies the oxbow through the downstream confluence and through the upstream underground paleochannel. Besides, the model attests to a non-negligible supply of the Auzon oxbow by the adjunct alluvial aquifer.

The current model can however be improved by completing the present hydrodynamic monitoring set with hydrological stations within the oxbow: one at the upstream ends of its downstream zone to compare data with the current hydrological station of the confluence; and one at the upstream end of the oxbow, close to the paleochannel water arrival. Flowrates measurements must indeed be performed in order to be able to quantify the water fluxes identified in this paper. Thus, the Auzon Oxbow role to manage flood events in the Allier River system would be evaluated. Besides, the impact of the Allier River arrival through the paleochannel on the water level of the upstream zone of the oxbow would be

Abbreviations: GW = groundwater; RB = right bank; LB = left bank; T = water temperature

assessed. Furthermore, such reliable conceptual models can be used for further applications: strategic wetlands operations or water quality managements responding to environmental and/or ecological issues. Indeed, such hydrodynamic knowledges on hydrosystems constitute an essential requirement to understand the transport of polluting substances by water. The conceptual hydrodynamic scheme coupled with the contaminants observations can support the assessment of the origin(s) and fate(s) of pollutants within wetlands hydrosystems and the identification of potential remediation processes occurences. The present conceptual model of the Auzon Oxbow hydrosystem is currently used to assess the role of that wetland regarding to excess nutrients and emerging molecules dynamics.

The study here proved that coupling several investigation approaches such as hydrodynamic (surface water and groundwater levels), geochemical (physico-chemical parameters and ionic concentrations) and isotopic (δ^2H-$\delta^{18}O$ of the water molecule) monitorings actually efficiently supports the identification of water supply sources to the wetland through space and time. Indeed, while the hydrodynamic approach gives general informations about surface water/grounwater interactions, the geochemical and

Abbreviations: GW = groundwater; RB = right bank; LB = left bank; T = water temperature

isotopic approaches complete the overview by identifying the origin of water, imaging the hydrochemistry of the oxbow and following the evolution of hydrodynamical and chemical parameters within time. Spatial and temporal disparities in the oxbow connection degree to the main stream and to the alluvial groundwater are proved to largely depend on river discharge during low and high flows. Besides, relevance of considering the degree of underground connection between the oxbow and the river was highlighted. The used of the multidisciplinary approach proposed here to image oxbows is then very promising.

Abbreviations: GW = groundwater; RB = right bank; LB = left bank; T = water temperature

Acknowledgments

The study was funded by the European Regional Development Fund (ERDF 2014-2020) through the CPER project “Les phytosanitaires du champ à l’assiette”. The authors also thank the Auvergne-Rhône-Alpes Region for its financial support. Besides, the study was carried out in an interdisciplinary setting under the aegis of the FR Environnement. Thanks also to the farmers of the study area who authorized the observation boreholes installation on their fields.

Abbreviations: GW = groundwater; RB = right bank; LB = left bank; T = water temperature

Sample ID		T	pH	EC	HCO_3^-	Cl^-	SO_4^{2-}	NO_3^-	NO_2^-	PO_4^{3-}	F^-	Na^+	Ca^{2+}	Mg^{2+}	K^+	NH_4^+	Li^+	δ^2H	$\delta^{18}O$
		(°C)		*(µS.cm^{-1})*							*(mg.l^{-1})*							*(‰ VSMOW)*	
Allier	Av.	12.3	7.6	110	30.2	9.9	6.1	3.2	0.0	0.1	0.1	7.1	7.7	3.2	1.6	0.1	0.0	-52.0	-8.0
	Min.	0.9	7.0	62	12.5	5.4	3.8	1.2	0.0	0.0	0.0	3.9	4.4	1.7	1.0	0.0	0.0	-56.7	-8.8
	Max.	21.8	8.8	152	49.0	14.7	10.3	6.7	0.0	0.1	0.3	9.6	11.8	4.9	2.6	0.2	0.0	-47.5	-7.1
	SD	6.0	0.4	17	7.8	2.0	1.3	1.4	0.0	0.0	0.0	1.2	1.5	0.7	0.3	0.0	0.0	3.4	0.6
B2	Av.	12.6	7.4	242	77.2	19.8	12.1	2.1	0.0	0.1	0.1	11.1	21.1	7.4	2.6	0.1	0.0	-51.4	-7.8
	Min.	1.1	6.9	76	16.7	6.6	5.0	0.2	0.0	0.0	0.1	4.7	5.1	2.0	1.5	0.0	0.0	-55.7	-8.6
	Max.	22.8	8.0	483	180.0	38.0	25.6	6.7	0.1	0.1	0.2	17.9	47.3	19.3	4.5	0.4	0.0	-47.4	-7.2
	SD	5.7	0.2	123	46.9	8.5	5.9	1.5	0.0	0.0	0.0	3.9	12.4	4.5	0.8	0.1	0.0	3.0	0.5
B2bis	Av.	12.3	7.2	362	116.1	31.6	17.2	1.9	0.0	0.1	0.2	16.0	34.0	10.2	4.0	0.1	0.0	-51.9	-7.9
	Min.	4.7	6.7	116	29.3	9.7	6.5	0.2	0.0	0.0	0.1	6.3	8.8	3.0	2.1	0.0	0.0	-52.9	-8.0
	Max.	18.4	7.9	452	151.0	48.7	31.4	8.0	0.1	0.1	0.3	20.5	48.3	15.9	20.7	0.2	0.0	-48.0	-7.5
	SD	3.9	0.2	63	24.1	8.2	5.1	1.8	0.0	0.0	0.0	2.9	7.8	2.3	2.9	0.1	0.0	1.6	0.2
B3	Av.	12.3	7.2	337	111.9	31.2	15.4	1.7	0.0	0.1	0.2	16.5	32.0	9.3	4.0	0.1	0.0	-52.6	-8.0
	Min.	5.5	6.8	140	42.0	12.6	7.4	0.2	0.0	0.0	0.1	7.8	11.1	3.5	2.7	0.0	0.0	-53.4	-8.1
	Max.	21.3	7.7	462	155.0	51.6	30.9	7.6	0.2	0.1	0.3	20.6	50.1	14.8	24.0	0.3	0.0	-52.0	-7.9
	SD	3.9	0.2	65	19.7	8.4	5.4	1.9	0.0	0.0	0.0	2.6	6.7	2.0	3.3	0.1	0.0	0.5	0.1
B4	Av.	12.3	7.1	337	111.1	30.4	14.9	1.9	0.0	0.1	0.2	16.5	31.8	9.1	3.5	0.1	0.0	-52.4	-7.9
	Min.	6.0	6.8	155	43.0	13.7	8.2	0.3	0.0	0.0	0.1	8.4	12.4	3.9	2.6	0.0	0.0	-53.2	-8.1
	Max.	20.9	7.9	425	133.0	44.6	25.9	7.6	0.1	0.2	0.3	20.8	40.5	11.7	4.1	0.3	0.0	-51.0	-7.7
	SD	3.3	0.2	57	17.1	7.4	4.3	1.8	0.0	0.0	0.0	2.6	6.0	1.6	0.3	0.1	0.0	0.8	0.2
B6	Av.	13.3	7.1	302	98.3	27.0	12.2	1.5	0.0	0.1	0.2	15.5	27.1	7.6	3.4	0.1	0.0	-52.5	-7.9
	Min.	6.6	6.7	210	53.0	17.0	7.3	0.1	0.0	0.0	0.1	11.4	16.4	5.3	2.7	0.0	0.0	-53.7	-8.2
	Max.	21.0	8.3	431	135.0	51.2	22.0	6.7	0.0	0.2	0.2	22.0	40.1	13.3	4.6	0.2	0.0	-50.8	-7.4
	SD	3.3	0.3	49	16.0	7.3	3.9	1.5	0.0	0.0	0.0	2.6	5.3	1.6	0.4	0.1	0.0	0.9	0.2
B7	Av.	12.8	7.0	215	69.7	19.3	8.4	2.3	0.0	0.1	0.1	12.2	18.7	5.1	2.7	0.1	0.0	-53.1	-8.1
	Min.	8.6	6.6	157	50.0	10.2	5.7	0.8	0.0	0.0	0.1	9.3	13.8	3.8	2.1	0.0	0.0	-54.8	-8.2
	Max.	18.3	7.6	373	95.0	28.8	13.5	9.0	0.0	0.5	0.2	16.5	25.8	6.8	5.0	0.2	0.0	-50.4	-7.7
	SD	2.0	0.2	37	10.0	5.1	2.0	1.5	0.0	0.1	0.0	1.9	2.6	0.7	0.5	0.1	0.0	1.3	0.2
Monteil	Av.	13.1	7.2	925	235.5	66.1	69.8	97.9	0.0	0.5	0.4	14.0	125.3	18.4	15.6	0.1	0.0	-50.0	-7.3
	Min.	9.5	7.0	871	134.0	55.1	60.8	87.0	0.0	0.0	0.3	12.3	74.1	16.8	10.6	0.0	0.0	-50.6	-7.5
	Max.	16.2	7.5	1031	273.0	97.3	87.3	120.6	0.1	4.1	0.6	18.4	145.6	25.1	47.0	0.3	0.0	-49.4	-7.2
	SD	1.7	0.1	39	26.9	9.3	4.7	7.5	0.0	0.6	0.1	1.2	13.5	1.5	7.7	0.1	0.0	0.4	0.1
P2	Av.	12.8	6.9	230	77.6	15.2	12.0	3.2	0.0	0.0	0.2	13.3	13.8	9.3	3.0	0.0	0.0	-54.8	-8.4
	Min.	4.9	6.5	147	34.0	8.5	3.1	0.0	0.0	0.0	0.1	7.7	7.5	5.4	1.4	0.0	0.0	-55.9	-8.6
	Max.	20.1	7.9	357	131.0	38.7	28.3	10.5	0.0	0.1	0.3	19.0	25.3	17.9	14.6	0.2	0.0	-54.0	-8.2
	SD	3.7	0.3	59	24.1	7.2	6.2	3.0	0.0	0.0	0.0	3.0	4.7	2.9	3.2	0.0	0.0	0.6	0.2
P3	Av.	12.5	7.1	744	238.5	53.1	61.0	26.0	0.0	0.1	0.3	17.3	80.8	28.2	4.2	0.0	0.0	-50.6	-7.6
	Min.	7.6	6.9	215	66.0	13.8	13.7	11.1	0.0	0.1	0.1	8.7	19.9	6.8	1.8	0.0	0.0	-51.2	-7.7
	Max.	17.3	7.4	950	293.0	101.0	105.0	46.1	0.1	0.7	0.4	23.5	102.1	39.8	7.0	0.2	0.0	-49.9	-7.5
	SD	2.5	0.2	101	34.1	12.9	12.1	6.8	0.0	0.1	0.1	2.1	13.9	4.4	0.7	0.0	0.0	0.4	0.1
P4	Av.	12.8	7.0	381	139.4	32.7	7.3	0.2	0.0	0.0	0.2	17.0	34.9	10.6	3.5	0.9	0.0	-52.1	-7.9
	Min.	5.1	6.7	287	101.0	21.7	0.1	0.0	0.0	0.0	0.1	13.0	26.1	7.5	2.5	0.1	0.0	-52.5	-8.0
	Max.	19.2	7.7	587	203.0	45.5	42.2	0.9	0.0	0.1	0.3	22.8	62.0	18.9	4.7	1.9	0.0	-51.4	-7.8
	SD	3.7	0.2	71	22.6	7.7	10.5	0.2	0.0	0.0	0.0	2.5	7.9	2.7	0.5	0.4	0.0	0.4	0.1
P5	Av.	12.6	7.1	795	255.4	59.8	65.3	20.4	0.0	0.2	0.2	20.0	87.9	29.1	3.1	0.0	0.0	-50.8	-7.6
	Min.	9.2	7.0	575	166.0	46.1	41.4	13.3	0.0	0.0	0.1	17.1	52.4	18.6	2.1	0.0	0.0	-51.6	-7.9
	Max.	15.5	7.7	859	295.0	70.0	73.8	34.4	0.1	0.8	0.3	23.1	104.0	39.0	4.8	0.1	0.0	-50.4	-7.5
	SD	1.8	0.1	48	26.0	5.8	5.2	5.2	0.0	0.2	0.0	1.3	12.9	2.7	0.4	0.0	0.0	0.4	0.1
P6	Av.	13.2	7.1	396	126.7	37.9	17.0	1.7	0.0	0.1	0.2	21.1	37.1	9.3	4.6	0.0	0.0	-53.1	-8.0
	Min.	5.7	6.7	253	74.0	21.0	9.3	0.0	0.0	0.0	0.1	14.6	24.0	6.0	2.5	0.0	0.0	-54.4	-8.3
	Max.	19.4	7.8	495	163.0	58.7	33.6	6.5	0.1	0.4	0.3	29.6	47.7	15.4	14.3	0.2	0.0	-52.0	-7.8
	SD	3.2	0.2	54	17.0	9.4	5.0	1.5	0.0	0.1	0.0	3.5	5.5	1.8	1.9	0.0	0.0	0.8	0.1
P7	Av.	13.3	6.9	219	69.5	20.6	8.2	2.4	0.0	0.3	0.2	12.9	19.1	5.2	3.2	0.0	0.0	-53.4	-8.2
	Min.	8.0	6.6	163	52.0	10.5	5.6	0.2	0.0	0.0	0.1	9.1	14.1	3.4	2.1	0.0	0.0	-54.7	-8.4
	Max.	20.5	7.7	316	91.0	48.5	12.9	7.5	0.1	0.8	0.2	18.9	24.2	9.5	23.5	0.1	0.0	-51.2	-7.8
	SD	2.5	0.3	34	9.1	8.0	1.9	1.4	0.0	0.2	0.0	2.5	2.5	1.1	3.4	0.0	0.0	1.1	0.2
P9	Av.	12.9	6.9	335	113.6	33.7	9.7	0.4	0.0	0.1	0.2	19.2	31.7	6.5	5.3	0.1	0.0	-53.3	-8.1
	Min.	6.6	6.6	203	70.0	15.9	3.9	0.0	0.0	0.0	0.2	11.1	19.7	4.2	2.6	0.0	0.0	-54.6	-8.5
	Max.	18.8	7.3	498	167.0	98.8	23.8	4.3	0.0	0.2	0.3	31.3	48.9	9.3	63.1	0.3	0.0	-51.3	-7.7
	SD	2.9	0.2	83	28.3	16.7	4.2	0.8	0.0	0.0	0.0	5.6	8.3	1.7	9.4	0.1	0.0	1.2	0.3
PZ1	Av.	13.1	7.1	290	95.8	28.3	11.3	0.8	0.0	0.1	0.2	16.3	27.3	6.4	4.0	0.1	0.0	-53.7	-8.1
	Min.	7.1	6.7	193	64.0	11.1	5.5	0.1	0.0	0.0	0.1	10.7	16.6	4.1	2.5	0.0	0.0	-57.7	-8.5
	Max.	19.1	7.6	413	131.0	82.0	35.1	4.0	0.0	0.2	0.3	25.5	43.9	10.4	25.1	0.2	0.0	-49.8	-7.5
	SD	2.8	0.2	73	18.4	15.4	6.8	1.0	0.0	0.0	0.0	3.9	7.7	1.9	3.5	0.1	0.0	1.7	0.3
PZ2	Av.	12.9	7.1	491	167.4	40.0	23.4	1.3	0.0	0.1	0.2	17.7	48.6	14.9	4.0	0.3	0.0	-52.0	-7.8
	Min.	7.2	6.8	325	114.0	24.2	4.8	0.1	0.0	0.0	0.1	13.0	30.6	8.9	2.8	0.0	0.0	-53.2	-8.1
	Max.	21.3	7.4	708	233.0	64.6	52.3	4.8	0.1	0.1	0.3	23.3	75.0	22.9	16.3	1.0	0.0	-50.8	-7.4
	SD	3.3	0.1	99	28.5	10.4	12.0	1.4	0.0	0.0	0.0	2.5	11.8	3.7	2.1	0.2	0.0	0.6	0.2
PZ3	Av.	13.2	7.3	861	300.0	68.7	62.8	3.2	0.0	0.1	0.2	22.8	94.3	29.5	4.5	0.1	0.0	-50.8	-7.4
	Min.	10.3	7.0	804	175.0	62.1	56.9	0.1	0.0	0.0	0.1	21.4	48.8	26.2	3.9	0.0	0.0	-51.8	-7.7
	Max.	17.8	7.7	1180	343.0	77.0	71.5	17.1	0.1	0.2	0.3	26.1	103.2	38.5	11.0	0.5	0.0	-50.0	-7.1
	SD	2.0	0.2	63	25.8	3.3	2.7	4.4	0.0	0.0	0.0	0.9	11.3	1.8	1.2	0.1	0.0	0.5	0.1
PZ4	Av.	13.3	7.2	782	275.1	51.3	57.0	12.3	0.0	0.1	0.2	18.0	81.8	32.5	5.0	0.1	0.0	-51.4	-7.6
	Min.	10.5	7.0	425	157.0	28.3	23.8	3.4	0.0	0.0	0.1	12.3	32.0	15.8	3.4	0.0	0.0	-53.2	-8.0
	Max.	17.6	7.6	1147	330.0	62.9	69.2	23.7	0.0	0.2	0.4	24.6	99.7	47.1	7.0	0.3	0.0	-50.0	-7.4
	SD	1.9	0.2	99	36.0	6.1	7.5	4.6	0.0	0.1	0.1	1.9	15.4	4.3	0.5	0.1	0.0	0.7	0.1
PZ5	Av.	12.9	7.3	938	335.9	68.2	76.1	4.7	0.0	0.1	0.2	20.0	110.6	33.7	6.9	0.1	0.0	-53.3	-7.9
	Min.	10.2	7.0	530	183.0	44.4	52.6	0.1	0.0	0.0	0.1	12.7	42.1	21.7	3.9	0.0	0.0	-55.6	-8.2
	Max.	17.6	7.7	1069	397.0	80.6	90.7	15.5	0.1	0.3	0.4	22.0	129.8	42.6	13.3	0.3	0.0	-49.2	-7.5
	SD	1.8	0.2	80	45.4	7.4	10.9	3.7	0.0	0.0	0.1	1.5	20.7	3.1	1.3	0.1	0.0	1.0	0.1
PZ6	Av.	11.8	7.4	1342	410.9	124.6	194.2	4.0	0.0	0.1	0.4	43.4	157.4	49.2	11.7	0.1	0.0	-51.9	-7.6
	Min.	8.1	7.1	1026	170.0	54.5	89.4	1.1	0.0	0.0	0.1	23.6	32.4	27.8	1.7	0.0	0.0	-53.0	-7.8
	Max.	15.3	7.6	3010	705.0	477.5	635.3	7.7	0.1	0.5	0.9	140.2	309.5	158.4	21.8	0.3	0.0	-49.1	-7.2
	SD	1.6	0.1	544	95.2	128.3	164.5	1.8	0.0	0.1	0.2	35.0	54.8	37.2	4.7	0.1	0.0	1.0	0.1

Abbreviations: GW = groundwater; RB = right bank; LB = left bank; T = water temperature

924 Table 1: Average, minimum, maximum and standard deviation (SD) values of physico-chemical parameters,
925 ions concentrations and $\delta^{18}O$-$\delta^{2}H$ data for the 40 campaigns carried out at the 21 samples sites of the
926 study zone.

927

928

Sample ID	T	pH	EC	HCO_3^-	Cl^-	SO_4^{2-}	NO_3^-	NO_2^-	PO_4^{3-}	F^-	Na^+	Ca^{2+}	Mg^{2+}	K^+	NH_4^+	Li^+
	(°C)		*(µS.cm^{-1})*						*(mg.l^{-1})*							
Allier	5.6	7.5	140	39.0	14.7	7.9	2.3	0.0	0.09	0.1	9.6	10.4	4.3	1.9	0.0	0.0
B2	6.7	7.4	218	62.0	20.3	11.8	1.9	0.0	0.11	0.1	11.5	19.4	6.8	2.4	0.0	0.0
B2bis	8.7	7.1	320	108.0	29.4	15.5	0.7	0.0	0.11	0.2	15.4	30.6	9.0	3.3	0.0	0.0
B3	8.5	7.0	314	113.0	29.3	14.7	0.6	0.0	0.08	0.2	15.7	29.9	8.7	3.5	0.0	0.0
B4	9.1	7.2	326	105.0	30.1	14.3	1.0	0.0	0.12	0.2	16.2	31.1	8.9	3.6	0.0	0.0
B6	10.3	7.0	243	81.0	22.9	11.6	1.4	0.0	0.11	0.2	12.8	22.4	6.9	2.8	0.0	0.0
B7	12.7	7.0	233	81.0	26.1	12.6	1.0	0.0	0.14	0.1	14.4	23.1	6.4	2.9	0.0	0.0
pt3	12.8	x	234	62.0	23.0	12.1	2.2	0.0	0.08	0.2	13.4	20.4	6.0	2.7	0.0	0.0
Monteil	12.6	7.1	872	226.0	57.5	64.3	95.0	0.1	0.15	0.5	12.5	123.8	17.1	11.0	0.0	0.0
P2	10.4	7.0	269	117.0	13.8	8.9	0.1	0.0	0.05	0.2	12.2	19.4	11.3	2.3	0.0	0.0
P3	11.6	7.1	776	243.0	60.4	73.4	27.2	0.0	0.14	0.3	17.7	89.4	29.0	4.4	0.1	0.0
P4	7.9	7.0	308	111.0	29.0	3.5	0.1	0.0	0.07	0.2	14.1	28.4	8.1	2.5	0.9	0.0
P5	11.9	7.2	811	265.0	65.9	66.4	25.5	0.0	0.09	0.3	20.5	95.3	29.1	3.2	0.1	0.0
P6	10.4	6.9	348	127.0	28.7	14.9	1.9	0.0	0.03	0.3	15.8	35.3	9.4	3.7	0.0	0.0
P7	12.5	6.6	245	74.0	25.6	10.8	1.2	0.0	0.08	0.1	14.6	22.9	6.6	2.6	0.0	0.0
P9	11.4	6.7	230	78.0	20.4	9.2	0.2	0.0	0.05	0.2	12.4	22.9	5.0	2.8	0.0	0.0
PZ1	12.6	7.0	197	82.0	16.0	6.4	0.1	0.0	0.08	0.2	11.1	19.0	4.5	2.6	0.0	0.0
PZ2	11.8	7.3	353	136.0	28.9	7.0	0.2	0.0	0.06	0.2	14.5	32.8	9.5	2.9	0.4	0.0
PZ3	13.0	7.1	855	308.0	69.9	61.5	3.0	0.0	0.12	0.2	22.5	98.0	29.4	4.2	0.1	0.0
PZ4	13.2	7.2	771	279.0	52.4	61.5	13.1	0.0	0.09	0.3	17.4	85.9	32.1	5.1	0.0	0.0
pt103	11.2	x	735	282.0	56.6	60.9	0.1	0.0	0.21	0.3	17.8	87.9	31.0	5.1	0.2	0.0
PZ5	13.2	7.3	1002	374.0	70.2	85.8	2.1	0.0	0.18	0.3	21.3	129.0	34.9	7.6	0.1	0.0
PZ6	12.1	7.3	1074	405.0	62.2	107.6	6.1	0.0	0.12	0.4	26.1	150.4	31.3	13.6	0.1	0.0

929

930 Table 2: Physico-chemical parameters and ions concentrations data for the 11/23-11/24/2017 campaign.

931

Abbreviations: GW = groundwater; RB = right bank; LB = left bank; T = water temperature

References

Alard, D., Bourcier, A., Bureau, F., Lefebvre, D., Mesnage, V., Poudevigne, I., 2001. Zones humides de la basse vallée de la Seine.

Amoros, C., Bornette, G., 2002. Connectivity and biocomplexity in waterbodies of riverine floodplains. Freshw. Biol. 47, 761–776. https://doi.org/10.1046/j.1365-2427.2002.00905.x

Andrade, A.I. a. S.S., Stigter, T.Y., 2011. Hydrogeochemical controls on shallow alluvial groundwater under agricultural land: case study in central Portugal. Environ. Earth Sci. 63, 809–825. https://doi.org/10.1007/s12665-010-0752-7

Archie, G.E., 1942. The Electrical Resistivity Log as an Aid in Determining Some Reservoir Characteristics. Transactions of the AIME 146, 54–62. https://doi.org/10.2118/942054-G

AUVERWATCH Database, 2018. AUVERWATCH Database [WWW Document]. https://doi.org/10.25519/AUVERWATCH-

Babka, B., Futó, I., Szabó, S., 2011. Clustering oxbow lakes in the Upper-Tisza Region on the basis of stable isotope measurements. J. Hydrol. 410, 105–113. https://doi.org/10.1016/j.jhydrol.2011.09.026

Abbreviations: GW = groundwater; RB = right bank; LB = left bank; T = water temperature

953 Banque Hydro [WWW Document], n.d. URL
954 http://hydro.eaufrance.fr/ (accessed 2.23.18).

955 Bates, B.C., Kundzewicz, Z.W., Wu, S., Palutikof, J.P., 2008.
956 IPCC Technical Paper VI, Climate Change and Water. IPCC
957 Secretariat, Geneva, Switzerland.

958 Beauger, A., 2008. Impact de la capture d'un chenal fluviatile
959 par une ancienne gravière sur la distribution des
960 macroinvertébrés benthiques. Rev. Sci. Eau J. Water Sci. 21,
961 87–98. https://doi.org/10.7202/017933ar

962 Beauger, A., Delcoigne, A., Voldoire, O., Serieyssol, K., Peiry, J.-
963 L., 2015. Distribution of Diatom, Macrophyte and Benthic
964 Macroinvertebrate Communities Related to Spatial and
965 Environmental Characteristics: The Example of a Cut-Off
966 Meander of the River Allier (France). Cryptogam. Algol. 36,
967 323–355. https://doi.org/10.7872/crya/v36.iss3.2015.323

968 Bengen, D., Lim, P., Belaud, A., 1992. Qualité des eaux de trois
969 bras morts de la Garonne : variabilité spatio-temporelle =
970 Water quality in three ancient arms of the river Garonne :
971 spatio-temporal variability. Rev. Sci. Eau FRA Hydrol. Cont. 5,
972 131–156.

973 Bornette, G., Amoros, C., Piegay, H., Tachet, J., Hein, T., 1998.
974 Ecological complexity of wetlands within a river landscape.

Abbreviations: GW = groundwater; RB = right bank; LB = left bank; T = water temperature

975 Biol. Conserv. 85, 35–45. https://doi.org/10.1016/S0006-
976 3207(97)00166-3

977 Bullock, A., Acreman, M., 2003. The role of wetlands in the
978 hydrological cycle. Hydrol. Earth Syst. Sci. Discuss. 7, 358–389.

979 Carrel, P.G., Juget, J., 1987. La Morte du Sauget, un ancien
980 méandre du Rhône: bilan hydrologique et biogéochimique.
981 Swiss J. Hydrol. 49, 102–125.
982 https://doi.org/10.1007/BF02540384

983 Celle-Jeanton, H., 2017. Projet RESEAU (AUVER-WATCH)
984 REseau de Suivi des Eaux en AUvergne (AUVERgne WATer
985 CHemsitry) (Rapport Final 2014-2016).

986 Chkirbene, A., Tsujimura, M., Cheref, A., Tanaka, T., 2009.
987 Hydro-geochemical evolution of groundwater in an alluvial
988 aquifer: Case of Kurokawa aquifer, Tochigi prefecture, Japan.
989 Desalination 246, 485–495.
990 https://doi.org/10.1016/j.desal.2008.04.057

991 Ciazela, J., Siepak, M., Wojtowicz, P., 2018. Tracking heavy
992 metal contamination in a complex river-oxbow lake system:
993 Middle Odra Valley, Germany/Poland. Science of The Total
994 Environment 616–617, 996–1006.
995 https://doi.org/10.1016/j.scitotenv.2017.10.219

Abbreviations: GW = groundwater; RB = right bank; LB = left bank; T = water temperature

Clark, I., Fritz, P., 1997. Environmental Isotopes in Hydrogeology.

Clay, A., Bradley, C., Gerrard, A.J., Leng, M.J., 2004. Using stable isotopes of water to infer wetland hydrological dynamics. Hydrol Earth Syst Sci 8, 1164–1173. https://doi.org/10.5194/hess-8-1164-2004

Craig, H., 1961. Isotopic Variations in Meteoric Waters. Science 133, 1702–1703. https://doi.org/10.1126/science.133.3465.1702

Dahl, T.E., 1990. Wetlands losses in the United States, 1780's to 1980's. U.S. Department of the Interior, Fish and Wildlife Service, Washington D.C. 13 pp.

Dahm, C.N., Grimm, N.B., Marmonier, P., Valett, H.M., Vervier, P., 1998. Nutrient dynamics at the interface between surface waters and groundwaters. Freshw. Biol. 40, 427–451. https://doi.org/10.1046/j.1365-2427.1998.00367.x

Davidson, N., 2014. How much wetland has the world lost? Long-term and recent trends in global wetland area. Mar. Freshw. Res. 65, 936–941. https://doi.org/10.1071/MF14173

Fontes, J.C., 1980. Environmental isotopes in groundwater hydrology. Handb. Environ. Isot. Geochem. Vol 1.

Abbreviations: GW = groundwater; RB = right bank; LB = left bank; T = water temperature

1017 Gagliano, S.M., Howard, P.C., 1984. The neck cutoff oxbow
1018 lake cycle along the Lower Mississippi River, in River
1019 meandering. Am. Soc. Civ. Eng. 147–158.

1020 Gay, A., 2015. Transfert de particules des versants aux masses
1021 d'eau sur le bassin Loire-Bretagne (thesis). Tours.

1022 Ghosh, D., Biswas, J.K., 2017. Catch per unit efforts and
1023 impacts of gears on fish abundance in an oxbow lake
1024 ecosystem in Eastern India. Environ. Health Eng. Manag. 4,
1025 169–175.

1026 Gleick, P.H., 1998. Water in Crisis: Paths to Sustainable Water
1027 Use. Ecol. Appl. 8, 571–579. https://doi.org/10.1890/1051-
1028 0761(1998)008[0571:WICPTS]2.0.CO;2

1029 Glińska-Lewczuk, K., 2009. Water quality dynamics of oxbow
1030 lakes in young glacial landscape of NE Poland in relation to
1031 their hydrological connectivity. Ecological Engineering 35, 25–
1032 37. https://doi.org/10.1016/j.ecoleng.2008.08.012

1033 Huang, Y., Zhou, Z., Wang, J., Dou, Z., Guo, Q., 2014. Spatial
1034 and temporal variability of the chemistry of the shallow
1035 groundwater in the alluvial fan area of the Luanhe river, North
1036 China. Environ. Earth Sci. 72, 5123–5137.
1037 https://doi.org/10.1007/s12665-014-3383-6

Abbreviations: GW = groundwater; RB = right bank; LB = left bank; T = water temperature

1038 Hudson, P.F., Heitmuller, F.T., Leitch, M.B., 2012. Hydrologic
1039 connectivity of oxbow lakes along the lower Guadalupe River,
1040 Texas: The influence of geomorphic and climatic controls on
1041 the “flood pulse concept.” J. Hydrol. 414–415, 174–183.
1042 https://doi.org/10.1016/j.jhydrol.2011.10.029

1043 Hulton, G., 2012. Global costs and benefits of drinking-water
1044 supply and sanitation interventions to reach the MDG target
1045 and universal coverage.

1046 Hunt, R., D. Bullen, T., Krabbenhoft, D., Kendall, C., 1998. Using
1047 Stable Isotopes of Water and Strontium to Investigate the
1048 Hydrology of a Natural and a Constructed Wetland. Ground
1049 Water 39, 271–293. https://doi.org/10.1111/j.1745-
1050 6584.1998.tb02814.x

1051 IAEA, 2009. Laser Spectroscopic Analysis of Liquid Water
1052 Samples for Stable Hydrogen and Oxygen Isotopes.

1053 Jubertie, F., 2006. Les excès climatiques dans le Massif Central
1054 français : l’impact des temps forts pluviométriques et
1055 anémométriques en Auvergne (thesis). Clermont-Ferrand 2.

1056 Kendall, C., McDonnell, J.J. (Eds.), 1999. Isotope Tracers in
1057 Catchment Hydrology. Elsevier Science, Amsterdam ; New
1058 York.

Abbreviations: GW = groundwater; RB = right bank; LB = left bank; T = water temperature

1059 Kolker, A.S., Cable, J.E., Johannesson, K.H., Allison, M.A., Inniss,
1060 L.V., 2013. Pathways and processes associated with the
1061 transport of groundwater in deltaic systems. J. Hydrol. 498,
1062 319–334. https://doi.org/10.1016/j.jhydrol.2013.06.014

1063 Korobova, E., Veldkamp, A., Ketner, P., Kroonenberg, S., 1997.
1064 Element partitioning in sediment, soil and vegetation in an
1065 alluvial terrace chronosequence, Limagne rift valley, France: A
1066 landscape geochemical study. CATENA 31, 91–117.
1067 https://doi.org/10.1016/S0341-8162(97)00029-5

1068 Larocque, M., Biron, P.M., Buffin-Bélanger, T., Needelman, M.,
1069 Cloutier, C.-A., McKenzie, J.M., 2016. Role of the geomorphic
1070 setting in controlling groundwater–surface water exchanges in
1071 riverine wetlands: A case study from two southern Québec
1072 rivers (Canada). Can. Water Resour. J. Rev. Can. Ressour. Hydr.
1073 1–15.

1074 Lasnier, B., Marchand, J., 1982. Brioude. Carte géologique de
1075 la France à 1/50 000.

1076 Le Coz, J., 2003. Réponse hydraulique d'un bras mort au signal
1077 hydrologique de la rivière.

1078 Loke, M.H., 2016. Tutorial : 2-D and 3-D electrical imaging
1079 surveys, IRIS Instruments.

Abbreviations: GW = groundwater; RB = right bank; LB = left bank; T = water temperature

Loke, M.H., 2011. Electrical Resistivity Surveys and Data Interpretation, in: Gupta, H.K. (Ed.), Encyclopedia of Solid Earth Geophysics. Springer Netherlands, Dordrecht, pp. 276–283. https://doi.org/10.1007/978-90-481-8702-7_46

Loke, M.H., Barker, R.D., 1996. Rapid least-squares inversion of apparent resistivity pseudosections by a quasi-Newton method1. Geophys. Prospect. 44, 131–152. https://doi.org/10.1111/j.1365-2478.1996.tb00142.x

Mohammed, N., 2014. Investigating the behavior of alluvial systems, thanks to the classical, isotopic and emerging tracers : case study of the alluvial aquifer of the Allier River (Auvergne, France). Bordeaux.

Mohammed, N., Celle-Jeanton, H., Huneau, F., Le Coustumer, P., Lavastre, V., Bertrand, G., Charrier, G., L. Clauzet, M., 2014. Isotopic and geochemical identification of main groundwater supply sources to an alluvial aquifer, the Allier River Valley (France). J. Hydrol. 508, 181–196. https://doi.org/10.1016/j.jhydrol.2013.10.051

Négrel, P., Petelet-Giraud, E., Widory, D., 2004. Strontium isotope geochemistry of alluvial groundwater: a tracer for groundwater resources characterisation. Hydrol Earth Syst Sci 8, 959–972. https://doi.org/10.5194/hess-8-959-2004

Abbreviations: GW = groundwater; RB = right bank; LB = left bank; T = water temperature

Négrel, Ph., Petelet-Giraud, E., Barbier, J., Gautier, E., 2003. Surface water–groundwater interactions in an alluvial plain: Chemical and isotopic systematics. J. Hydrol. 277, 248–267. https://doi.org/10.1016/S0022-1694(03)00125-2

Ounaïes, S., Schäfer, G., Trémolières, M., 2013. Quantification of vertical water fluxes in the vadose zone using particle-size distribution and pedology-based approaches to model soil heterogeneities. Hydrol. Process. 27, 2306–2324. https://doi.org/10.1002/hyp.9365

Pastre, J.F., 1986. Altération et paléoaltération des minéraux lourds des alluvions pliocenes et pleistocenes du bassin de l'Allier (Massif central, France). Quaternaire 23, 257–269. https://doi.org/10.3406/quate.1986.1821

Penna, D., B, S., Sanda, M., S, W., Bogaard, T., A, G., Borga, M., M. C. Fischer, B., M, B., Z, C., 2010. On the reproducibility and repeatability of laser absorption spectroscopy measurements for ??2H and ??18O isotopic analysis. Hydrol. Earth Syst. Sci. Discuss. 14. https://doi.org/10.5194/hess-14-1551-2010

Petelet-Giraud, E., Casanova, J., Chery, L., Negrel, P., Bushaert, S., 2005. Essai de caractérisation isotopique (δ18O et δ2H) du signal metéorique actuel à partir des lacs et réservoirs :

Abbreviations: GW = groundwater; RB = right bank; LB = left bank; T = water temperature

application au quart sud-ouest de la France. Houille Blanche 57–62. https://doi.org/10.1051/lhb:200502008

PNMH, 2014. 3rd National Action Plan for Wetlands (2014-2018). Ministère de l'Écologie, du Développement durable et de l'Énergie, La Défense, France.

PREVISIONS METEO FRANCE - Site Officiel de Météo-France - Prévisions gratuites à 15 jours sur la France et à 10 jours sur le monde [WWW Document], n.d. URL http://www.meteofrance.com/accueil (accessed 2.14.18).

Rathore, V.S., Nathawat, M.S., Champatiray, P.K., 2010. Palaeochannel detection and aquifer performance assessment in Mendha River catchment, Western India. J. Hydrol. 395, 216–225. https://doi.org/10.1016/j.jhydrol.2010.10.026

Rollet, A.J., Citterio, A., Dufour, S., Lejot, J., Piegay, H., 2005. Expertise hydro-géomorphologique en vue du diagnostic fonctionnel des habitas, de la restauration du transit sédimentaire et des lônes, volet 1, 2, 3 et 4.

Roux, J.-C., 2006. AQUIFERES ET EAUX SOUTERRAINES DE FRANCE-COFFRET 2 TOME. BRGM, Orléans.

Rozanski, K., Froehlich, K., Mook, W.G., 2001. Environmental isotopes in the hydrological cycle: principles and applications. Volume 3: surface water. IHP-V Tech. Doc. Hydrol. No 39.

Abbreviations: GW = groundwater; RB = right bank; LB = left bank; T = water temperature

Rudel, A., 1963. Les minéraux lourds des terrasses Quaternaires de Limagne d'Auvergne et leséruptions montdoriennes. Soc Géol Fr Bull 7, 468–469.

Sarris, T.S., Close, M., Abraham, P., 2018. Using solute and heat tracers for aquifer characterization in a strongly heterogeneous alluvial aquifer. J. Hydrol. 558, 55–71. https://doi.org/10.1016/j.jhydrol.2018.01.032

Sinha, R., Yadav, G.S., Gupta, S., Singh, A., Lahiri, S.K., 2013. Geo-electric resistivity evidence for subsurface palaeochannel systems adjacent to Harappan sites in northwest India. Quat. Int., Geoarchaeology: a toolbox of approaches applied in a multidisciplinary research discipline 308–309, 66–75. https://doi.org/10.1016/j.quaint.2012.08.002

Sutton, M.A., Bleeker, A., Howard, C.M., Bekunda, M., Grizzetti, B., de Vries, W., van Grinsven, H.J.M., Abrol, Y.P., Adhya, T.K., Billen, G., Davidson, E.A., Datta, A., Diaz, R., Erisman, J.W., Liu, X.J., Oenema, O., Palm, C., Raghuram, N., Reis, S., Scholz, R.W., Sims, T., Westhoek, H., Zhang, F.S., 2013. Our nutrient world: the challenge to produce more food and energy with less pollution. NERC/Centre for Ecology & Hydrology, Edinburgh.

Abbreviations: GW = groundwater; RB = right bank; LB = left bank; T = water temperature

Teles, V., Delay, F., de Marsily, G., 2004. Comparison of genesis and geostatistical methods for characterizing the heterogeneity of alluvial media: Groundwater flow and transport simulations. J. Hydrol., Stochastic Models of Flow and Transport in Multiple-scale Heterogeneous Porous Media 294, 103–121. https://doi.org/10.1016/j.jhydrol.2003.11.041

Tockner, K., Schiemer, F., Baumgartner, C., Kum, G., Weigand, E., Zweimüller, I., Ward, J.V., 1999. The Danube restoration project: species diversity patterns across connectivity gradients in the floodplain system. Regulated Rivers: Research & Management 15, 245–258. https://doi.org/10.1002/(SICI)1099-1646(199901/06)15:1/3<245::AID-RRR540>3.0.CO;2-G

UNEP, 2016. A Snapshot of the World's Water Quality: Towards a global assessment. United Nations Environment Programme, Nairobi, Kenya.

Vanderhaeghe, O., Prognon, F., 2012. Saint-Germain-Lembron. Carte géologique de la France à 1/50 000.

Veldkamp, E., Jongmans, A.G., 1990. Weathering of alcali basalt gravel in two older Allier river terraces, Limagne, France. Chem. Geol., Geochemistry of the earth's surface and

Abbreviations: GW = groundwater; RB = right bank; LB = left bank; T = water temperature

of mineral formation 84, 148–149. https://doi.org/10.1016/0009-2541(90)90193-B

Ward, J.V., Tockner, K., Arscott, D.B., Claret, C., 2002. Riverine landscape diversity. Freshwater Biology 47, 517–539. https://doi.org/10.1046/j.1365-2427.2002.00893.x

Winter, T.C., Harvey, J.W., Franke, O.L., Alley, W.M., 1998. Ground water and surface water; a single resource (USGS Numbered Series No. 1139), Circular. U.S. Geological Survey,.

Wren, D.G., Davidson, G.R., Walker, W.G., Galicki, S.J., 2008. The evolution of an oxbow lake in the Mississippi alluvial floodplain. J. Soil Water Conserv. 63, 129–135. https://doi.org/10.2489/jswc.63.3.129

Yang, C., Cai, X., Wang, X., 2018. Remote Sensing of Hydrological Changes in Tian-e-Zhou Oxbow Lake, an Ungauged Area of the Yangtze River Basin. Remote Sens. 10, 1-N.PAG. https://doi.org/10.3390/rs10010027

Abbreviations: GW = groundwater; RB = right bank; LB = left bank; T = water temperature

List of Figures

22 area highlights the decrease of EC during the April 2016 campaign
23 in the Auzon Oxbow and PZ4.

24 Figure 5: Chemical water types of the 21 sampling sites given by a
25 Piper's diagram established from data in $mg.l^{-1}$.

26 Figure 6: HCO_3^- vs Na^+/Ca^{2+} ($mg.l^{-1}$) for Allier River, RB GW (mean
27 of P2, P4, P6, P7, P9, PZ1 and PZ2), LB GW (mean of P3, P5, PZ3,
28 PZ4, PZ5 and PZ6), Auzon Oxbow (B2 to B7) and Le Monteil Spring.
29 The dashed line is an indicative mixing line between Allier River
30 and LB GW end-members which explain the Auzon Oxbow
31 signatures.

32 Figure 7: Cartography of EC performed on the 11/23/2017.

33 Figure 8: Piper's diagram established from data in $mg.l^{-1}$ of the 21
34 sampling sites and of the two water arrivals (Pt 3 and 103)
35 analyzed for the 11/23-24/17 campaign.

36 Figure 9: ERT profile crossing the active paleochannel (blue circle)
37 upstream from the Auzon Oxbow (orientation SSE-NNW).

38 Figure 10: a) $\delta^{18}O$ time-series for Allier River and Auzon Oxbow
39 (DZ: B2bis; IZ: B4; UZ: B7) from April to November 2017; b) $\delta^{2}H$
40 and $\delta^{18}O$ signatures for Allier River, RB GW (mean of P2, P4, P6,
41 P7, P9, PZ1 and PZ2), LB GW (mean of P3, P5, PZ3, PZ4, PZ5 and

PZ6), Auzon Oxbow (B2 to B7) and Le Monteil spring. Local Meteoric Water Line (LMWL: $\delta^2H = 8* \delta^{18}O + 13.7‰$ by Petelet-Giraud et al. (2005)) and Global Meteoric Water Line (GMWL: $\delta^2H = 8* \delta^{18}O + 10‰$ by Craig (1961)) are also shown for comparison.

Figure 11: Conceptual model of the Auzon Oxbow: identification of its interactions with the Allier River and the alluvial aquifer. The river supplies its annex by the surface connection at the downstream confluence and by an underground connection through the upstream paleochannel (which recharge during HF). The alluvial groundwater of the left bank was identified to supply the oxbow during LF especially in its downstream part.

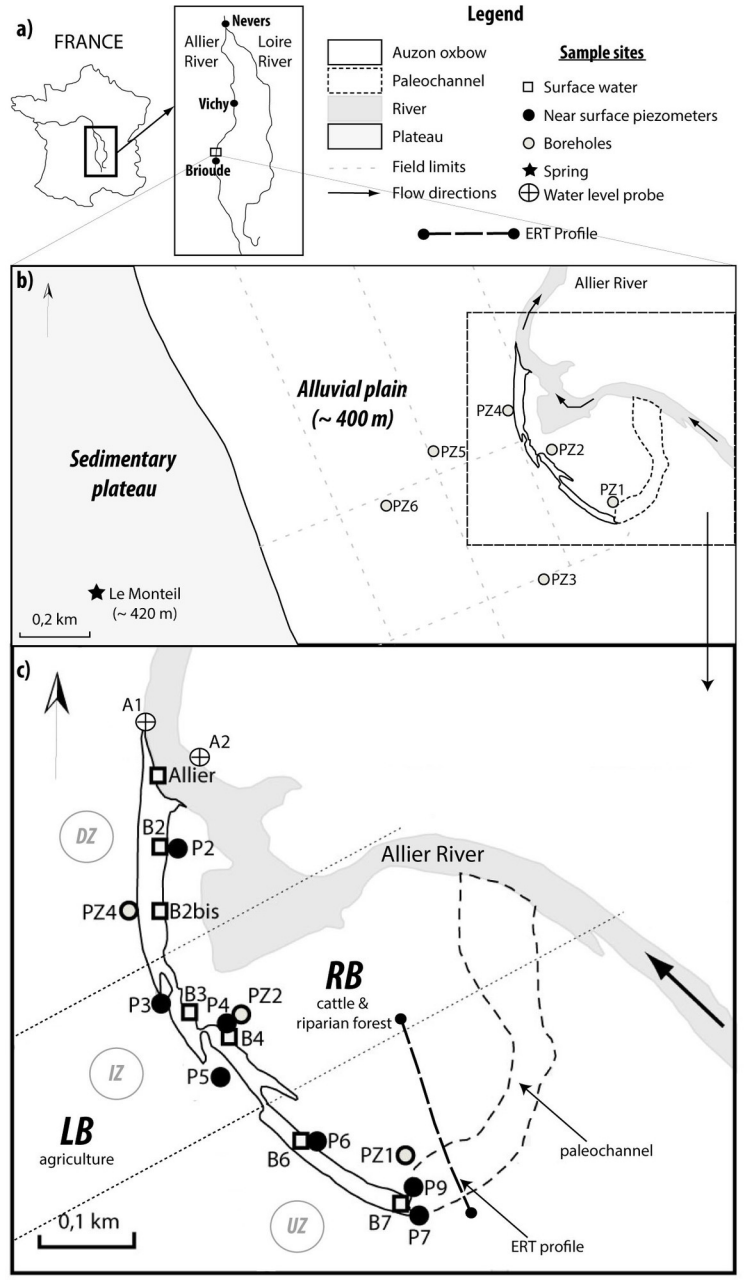
a)
FRANCE
Nevers
Allier River
Loire River
Vichy
Brioude
Legend
Auzon oxbow
Paleochannel
River
Plateau
Field limits
Flow directions
Sample sites
Surface water
Near surface piezometers
Boreholes
Spring
Water level probe
ERT Profile
b)
Allier River
Alluvial plain (~ 400 m)
Sedimentary plateau
PZ4
PZ5
PZ2
PZ1
PZ6
PZ3
Le Monteil (~ 420 m)
0,2 km
c)
A1
A2
Allier
DZ
B2
P2
Allier River
PZ4
B2bis
RB
cattle & riparian forest
P3
B3
P4
PZ2
B4
IZ
P5
LB
agriculture
P6
B6
PZ1
P9
B7
P7
paleochannel
ERT profile
0,1 km
UZ

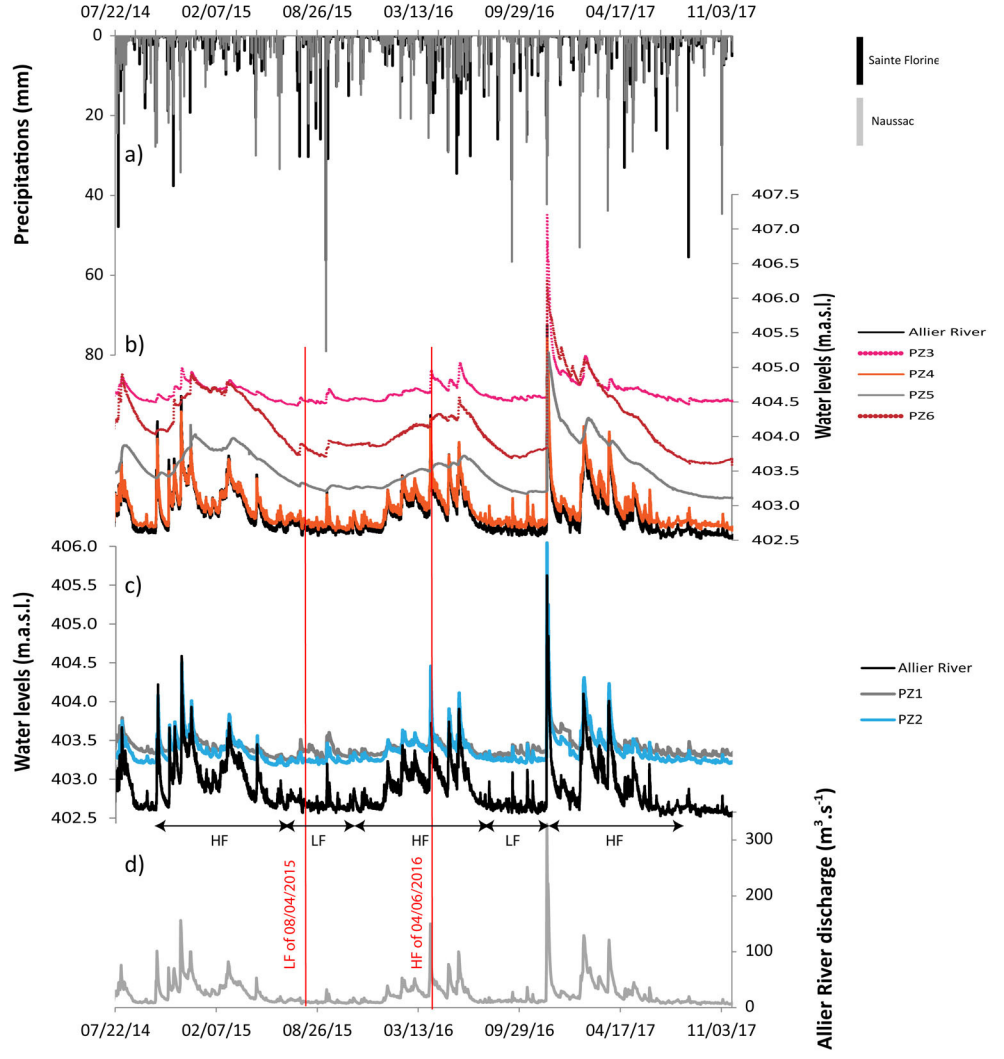
07/22/14
02/07/15
08/26/15
03/13/16
09/29/16
04/17/17
11/03/17
Precipitations (mm)
0
20
40
60
80
a)
Sainte Florine
Naussac
b)
Water levels (m.a.s.l.)
407.5
407.0
406.5
406.0
405.5
405.0
404.5
404.0
403.5
403.0
402.5
Allier River
PZ3
PZ4
PZ5
PZ6
c)
Water levels (m.a.s.l.)
406.0
405.5
405.0
404.5
404.0
403.5
403.0
402.5
Allier River
PZ1
PZ2
HF
LF
HF
LF
HF
d)
LF of 08/04/2015
HF of 04/06/2016
Allier River discharge (m³.s⁻¹)
300
200
100
0
07/22/14
02/07/15
08/26/15
03/13/16
09/29/16
04/17/17
11/03/17

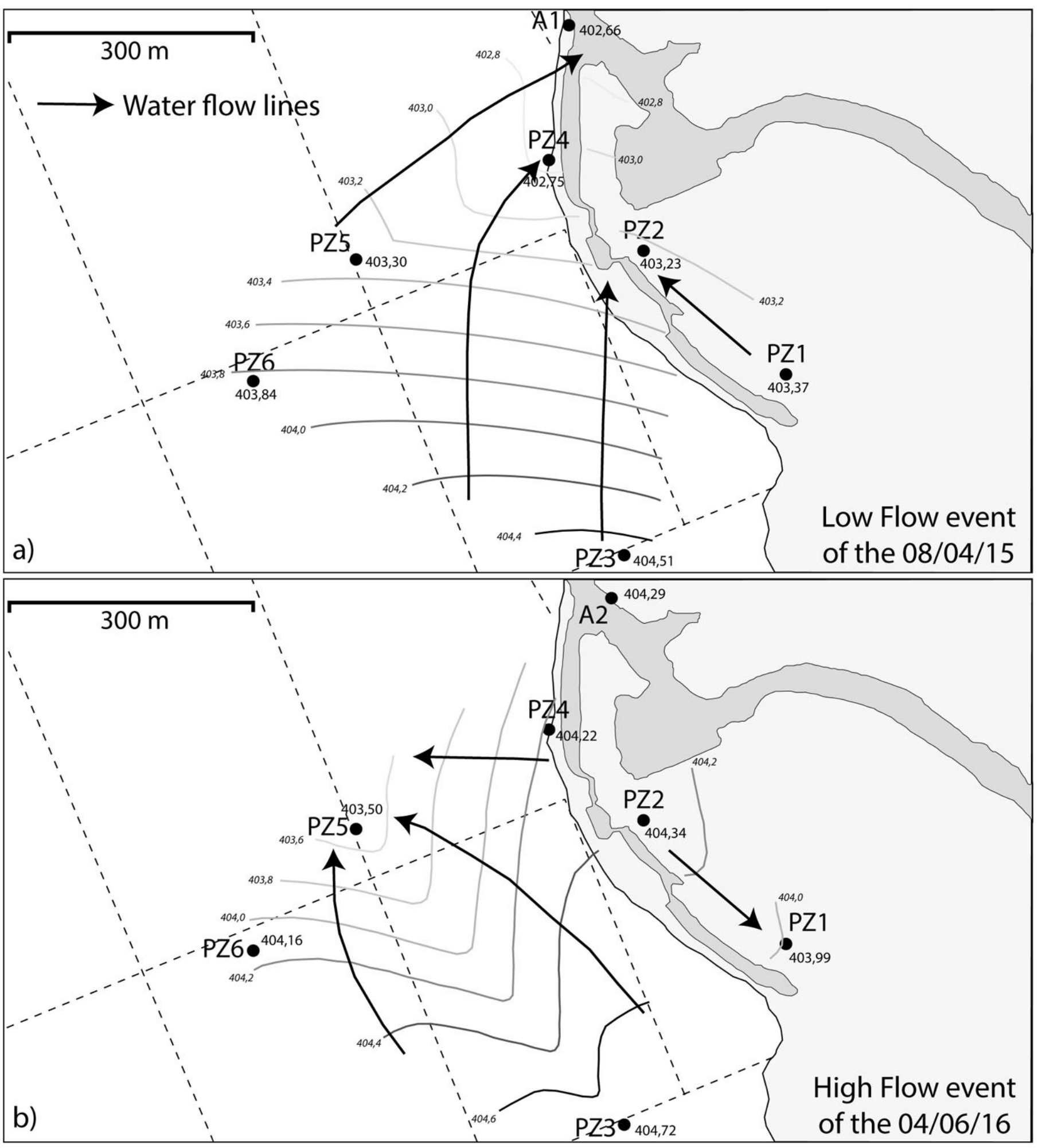
300 m
Water flow lines
A1
402,66
402,8
403,0
PZ4
402,75
403,2
PZ5
403,30
403,4
403,6
PZ6
403,8
403,84
404,0
404,2
PZ2
403,23
403,2
PZ1
403,37
404,4
PZ3
404,51
a)
Low Flow event
of the 08/04/15
300 m
404,29
A2
PZ4
404,22
404,2
PZ2
404,34
403,50
PZ5
403,6
403,8
404,0
PZ6
404,16
404,2
404,0
PZ1
403,99
404,4
404,6
PZ3
404,72
b)
High Flow event
of the 04/06/16

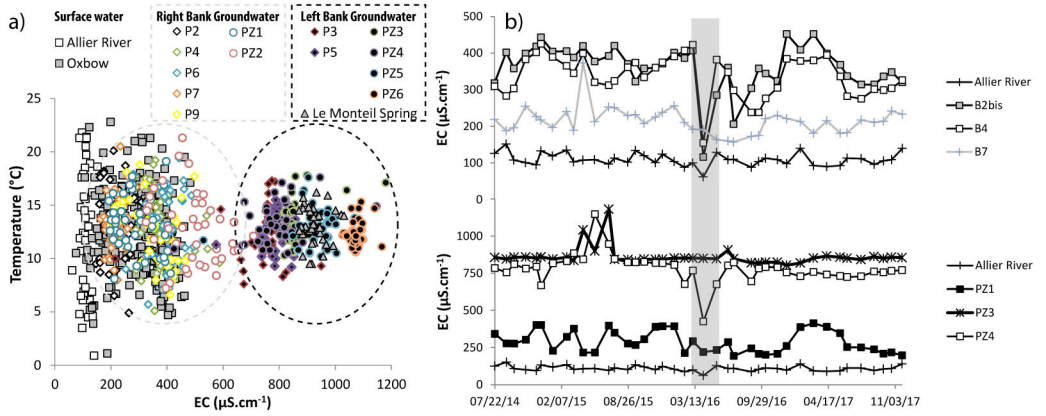
a)
Surface water
Allier River
Oxbow
Right Bank Groundwater
P2
P4
P6
P7
P9
PZ1
PZ2
Left Bank Groundwater
P3
P5
PZ3
PZ4
PZ5
PZ6
Le Monteil Spring
Temperature (°C)
EC (µS.cm-1)
b)
EC (µS.cm-1)
Allier River
B2bis
B4
B7
EC (µS.cm-1)
Allier River
PZ1
PZ3
PZ4
07/22/14
02/07/15
08/26/15
03/13/16
09/29/16
04/17/17
11/03/17

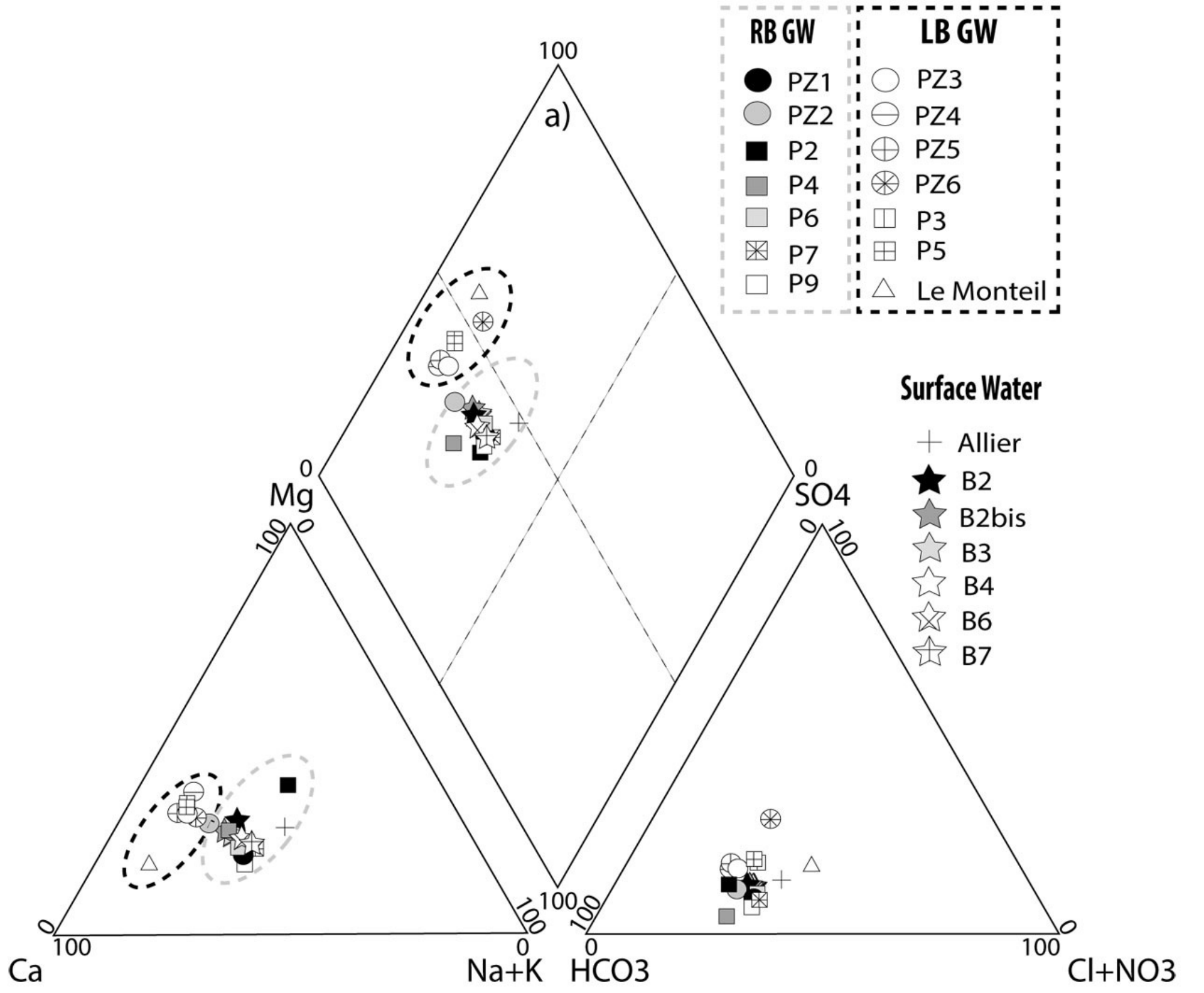
RB GW
PZ1
PZ2
P2
P4
P6
P7
P9
LB GW
PZ3
PZ4
PZ5
PZ6
P3
P5
Le Monteil
a)
Surface Water
Allier
B2
B2bis
B3
B4
B6
B7
100
0
Mg
SO4
Ca
Na+K
HCO3
Cl+NO3

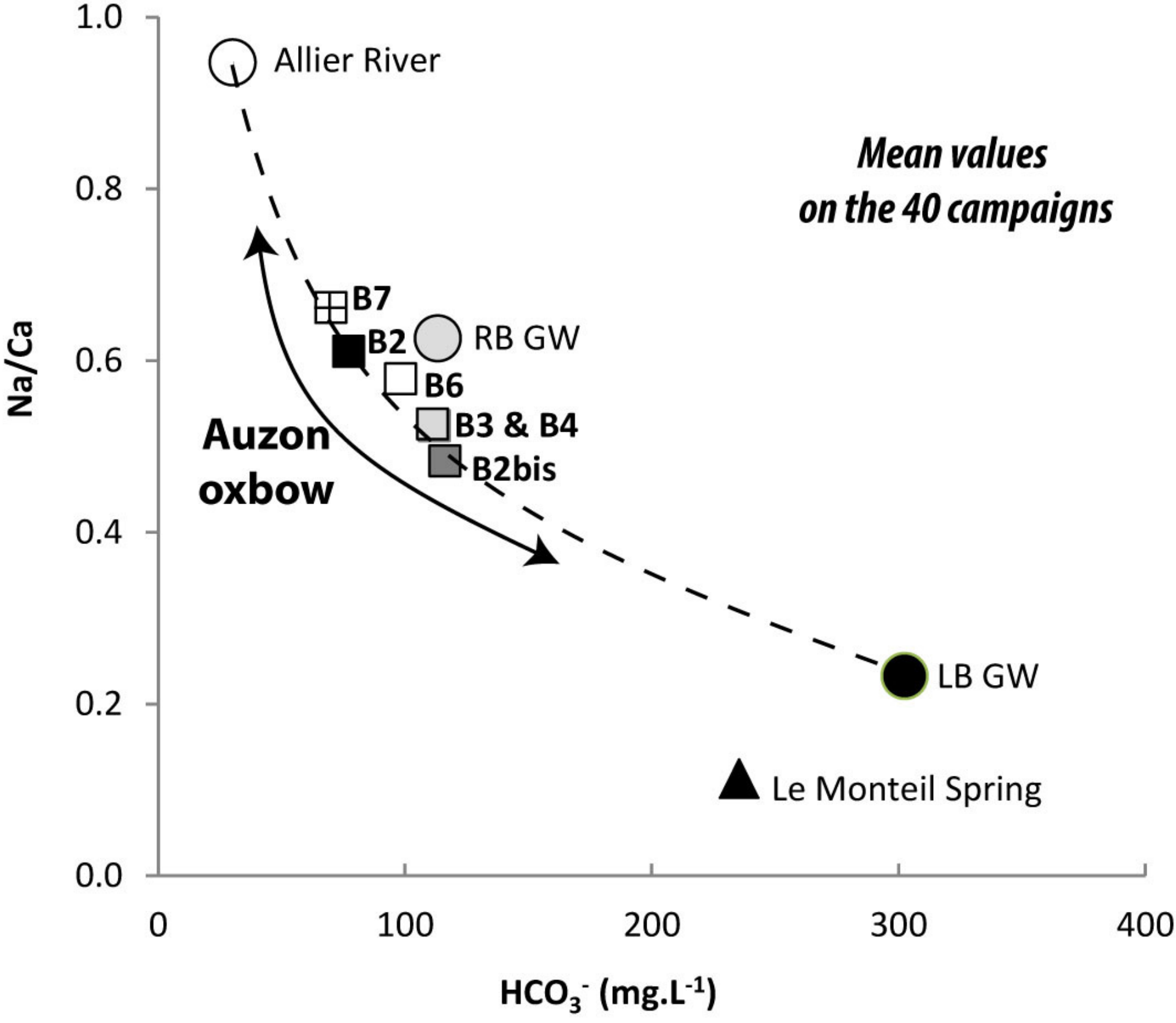
1.0
0.8
0.6
0.4
0.2
0.0
Na/Ca
0
100
200
300
400
HCO3- (mg.L-1)
Allier River
Mean values
on the 40 campaigns
B7
B2
RB GW
B6
B3 & B4
B2bis
Auzon
oxbow
LB GW
Le Monteil Spring

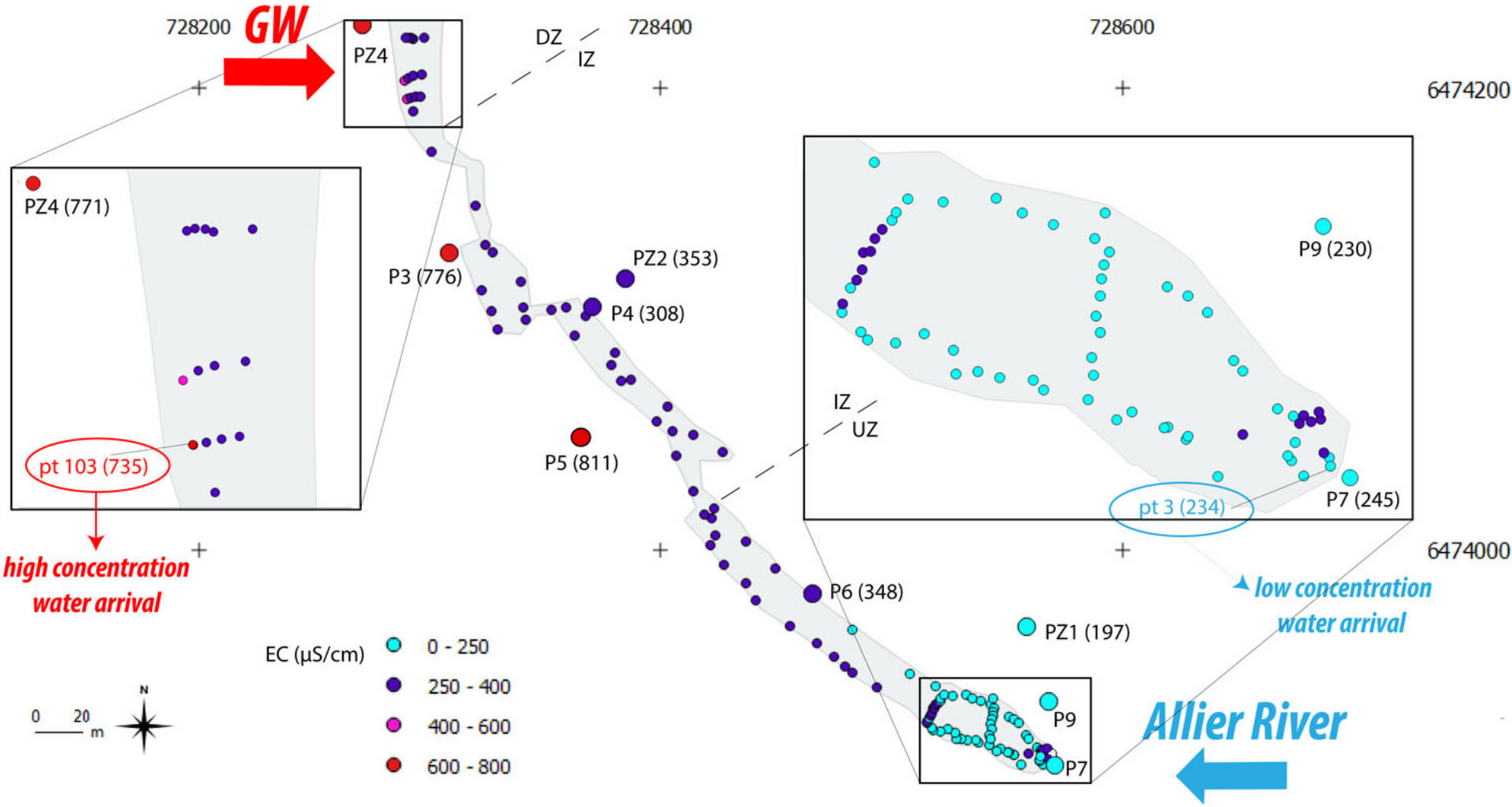
728200
GW
PZ4
DZ
IZ
728400
728600
6474200
PZ4 (771)
P3 (776)
PZ2 (353)
P4 (308)
P9 (230)
IZ
UZ
P5 (811)
pt 103 (735)
P7 (245)
pt 3 (234)
6474000
high concentration
water arrival
low concentration
water arrival
P6 (348)
PZ1 (197)
EC (µS/cm)
0 - 250
250 - 400
400 - 600
600 - 800
P9
P7
Allier River
0
20
m
N

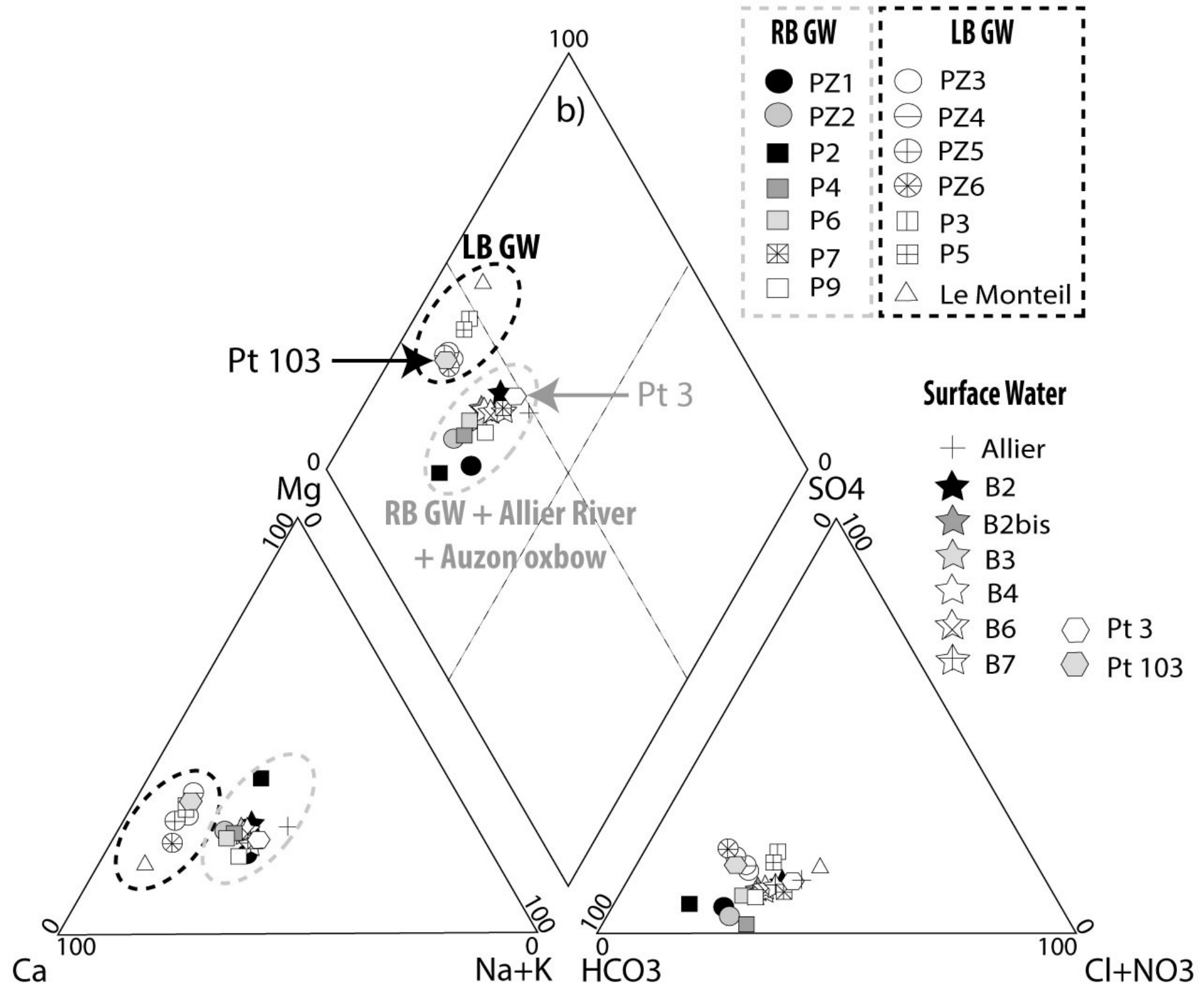
RB GW
PZ1
PZ2
P2
P4
P6
P7
P9
LB GW
PZ3
PZ4
PZ5
PZ6
P3
P5
Le Monteil
b)
LB GW
Pt 103
Pt 3
RB GW + Allier River
+ Auzon oxbow
Surface Water
Allier
B2
B2bis
B3
B4
B6
B7
Pt 3
Pt 103
100
0
Mg
SO4
Ca
Na+K
HCO3
Cl+NO3

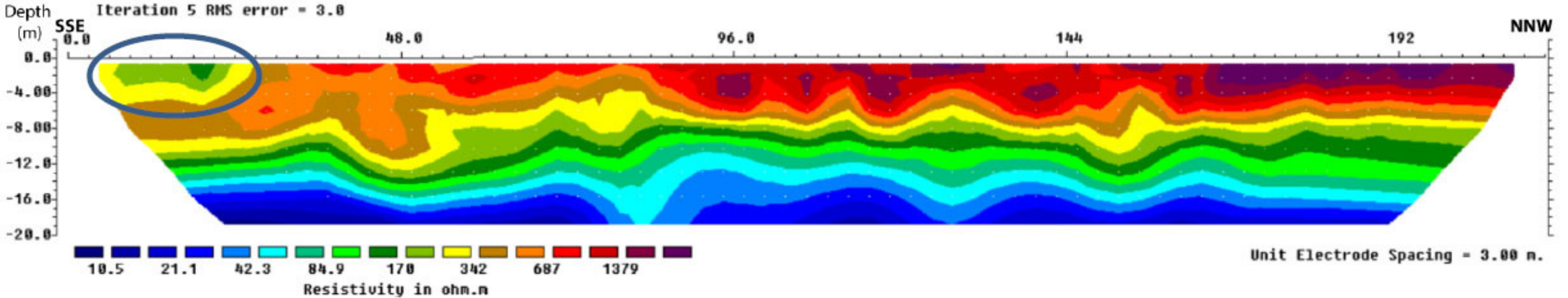
Depth
(m)
Iteration 5 RMS error = 3.0
SSE
NNW
0.0
48.0
96.0
144
192
0.0
-4.00
-8.00
-12.0
-16.0
-20.0
10.5
21.1
42.3
84.9
170
342
687
1379
Resistivity in ohm.m
Unit Electrode Spacing = 3.00 m.

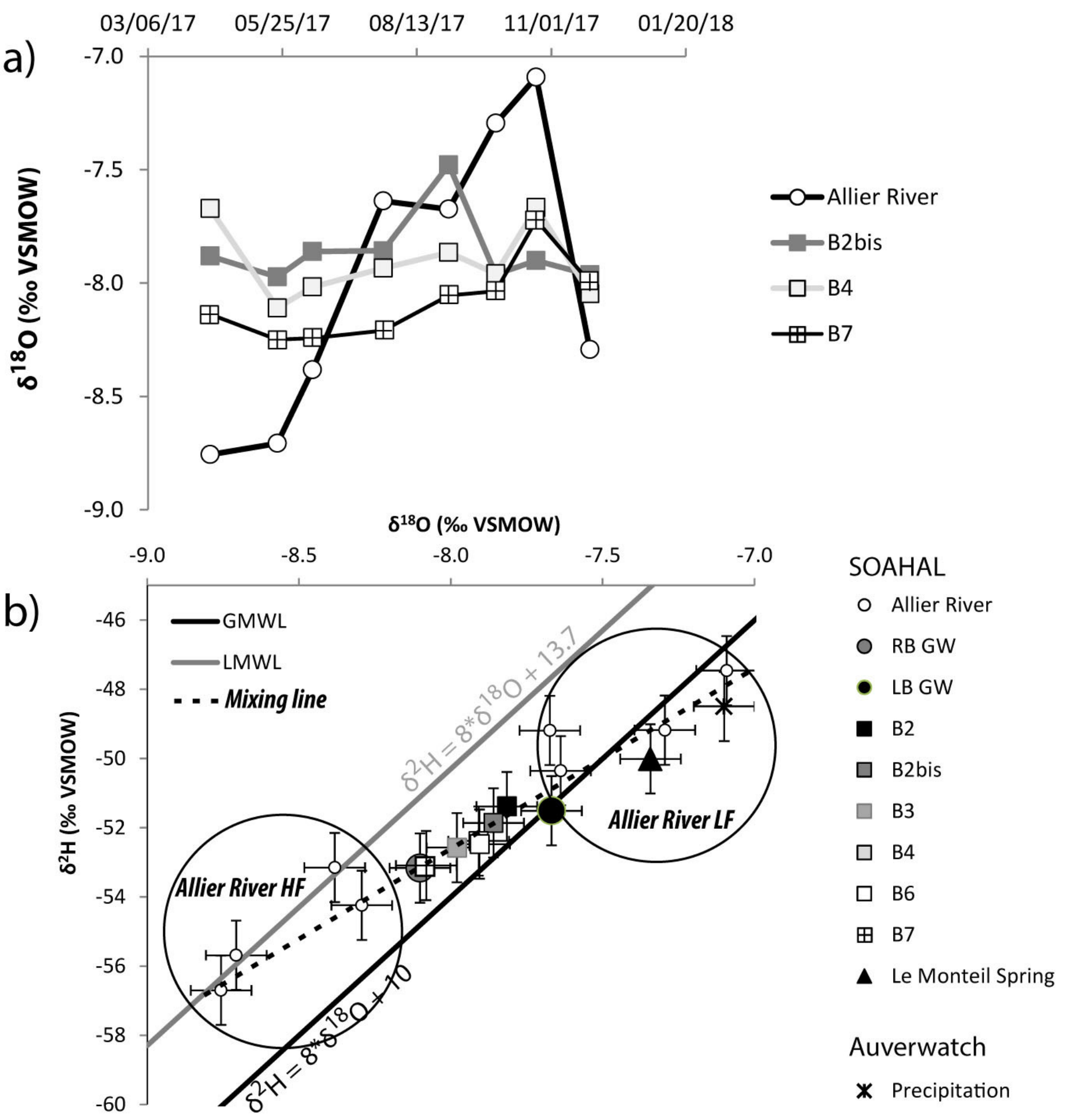
a)
03/06/17
05/25/17
08/13/17
11/01/17
01/20/18
-7.0
-7.5
-8.0
-8.5
-9.0
δ18O (‰ VSMOW)
Allier River
B2bis
B4
B7
b)
δ18O (‰ VSMOW)
-9.0
-8.5
-8.0
-7.5
-7.0
δ2H (‰ VSMOW)
-46
-48
-50
-52
-54
-56
-58
-60
GMWL
LMWL
Mixing line
δ2H = 8*δ18O + 13.7
δ2H = 8*δ18O + 10
Allier River HF
Allier River LF
SOAHAL
Allier River
RB GW
LB GW
B2
B2bis
B3
B4
B6
B7
Le Monteil Spring
Auverwatch
Precipitation

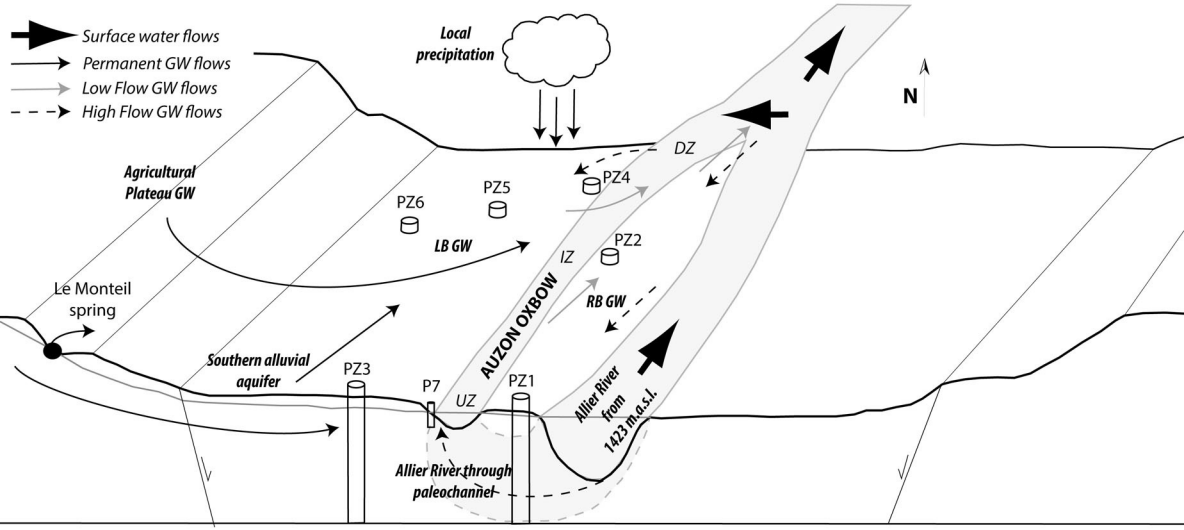
Surface water flows
Permanent GW flows
Low Flow GW flows
High Flow GW flows
Local precipitation
N
DZ
PZ4
PZ5
PZ6
Agricultural Plateau GW
LB GW
IZ
PZ2
RB GW
AUZON OXBOW
Le Monteil spring
Southern alluvial aquifer
PZ3
P7
UZ
PZ1
Allier River from 1423 m.a.s.l.
Allier River through paleochannel